Robotica (2017) volume 35, pp. 1006–1030. © Cambridge University Press 2015
doi:10.1017/S0263574715000934

Closed form Newton–Euler dynamic model of flexible manipulators

Luca Bascetta†, Gianni Ferretti†* and Bruno Scaglioni†‡

†*Politecnico di Milano, Dipartimento di Elettronica, Informazione e Bioingegneria Piazza Leonardo da Vinci 32, 20133, Milano, Italy. E-mail: luca.bascetta@polimi.it*
‡*MUSP Lab, Via Tirotti 9, Le Mose, 29122 Piacenza, Italy. E-mail: bruno.scaglioni@polimi.it*

(Accepted October 15, 2015. First published online: November 17, 2015)

SUMMARY
In this paper, a closed-form dynamic model of flexible manipulators is developed, based on the Newton–Euler formulation of motion equations of flexible links and on the adoption of the spatial vector notation. The proposed model accounts for two main innovations with respect to the state of the art: it is obtained in closed form with respect to the joints and modal coordinates (including the quadratic velocity terms) and motion equations of the whole manipulator can be computed for any arbitrary shape of the links and any possible link cardinality starting from the output of several commercial (finite element analysis) FEA codes. The Newton–Euler formulation of motion equations in terms of the joint and elastic variables greatly improves the simulation performances and makes the model suitable for real-time control and active vibration damping. The model has been compared with literature benchmarks obtained by the classical multibody approach and further validated by comparison with experiments collected on an experimental manipulator.

KEYWORDS: Flexible manipulators; Flexible multibody systems; Robotics; Dynamics; Simulation.

Nomenclature

N	Number of joints
M_i	Number of modal coordinates of link i
$M = \sum_{i=1}^{N} M_i$	Total number of modal coordinates
θ_i	Coordinate of the joint connecting link i to link $i-1$
$\boldsymbol{\theta} = \text{col}\{\theta_i\} \in \mathbb{R}^N$	Global vector of joint coordinates
$\boldsymbol{q}_i \in \mathbb{R}^{M_i}$	Vector of modal coordinates of link i
$\boldsymbol{q} = \text{col}\{\boldsymbol{q}_i\} \in \mathbb{R}^M$	Global vector of modal coordinates
τ_i	Torque acting on the joint connecting link i to link $i-1$
$\boldsymbol{\tau} = \text{col}\{\tau_i\} \in \mathbb{R}^N$	Global vector of joint torques
$\{O_i, \boldsymbol{x}_i, \boldsymbol{y}_i, \boldsymbol{z}_i\}$	Local Floating Frame of Reference (FFR) attached to link i
$\{O'_i, \boldsymbol{x}'_i, \boldsymbol{y}'_i, \boldsymbol{z}'_i\}$	Local reference frame having the same orientation of the FFR frame in the undeformed configuration and with the origin O'_i coinciding with the origin O_{i+1} of the FFR of the next link in the chain
$\hat{\boldsymbol{z}}'_{i-1} \in \mathbb{R}^3$	Axis of rotation of the joint connecting link i to link $i-1$ expressed in the reference frame $\{O'_{i-1}, \boldsymbol{x}'_{i-1}, \boldsymbol{y}'_{i-1}, \boldsymbol{z}'_{i-1}\}$
$\boldsymbol{p}_i \in \mathbb{R}^3$	Position of the origin O_i of the ith frame with respect to the origin of the world frame expressed in the world frame
$\boldsymbol{p}_{i+1,i} \in \mathbb{R}^3$	Position of the origin O_{i+1} of the $(i+1)$th frame with respect to the origin O_i of the ith frame, in the world frame

* Corresponding author. E-mail: gianni.ferretti@polimi.it

https://doi.org/10.1017/S0263574715000934 Published online by Cambridge University Press

$\boldsymbol{A}_i \in \mathbb{R}^{3\times 3}$	Rotation matrix relating the FFR and the world reference frame
$\bar{\boldsymbol{u}}_i \in \mathbb{R}^3$	Position of the origin O_{i+1} of the $(i+1)$th frame with respect to the origin O_i of the ith frame, in the $\{O_i, \boldsymbol{x}_i, \boldsymbol{y}_i, \boldsymbol{z}_i\}$ frame
$\bar{\boldsymbol{u}}_{0,i} \in \mathbb{R}^3$	Position of the origin O_{i+1} of the $(i+1)$th frame with respect to the origin O_i of the ith frame, in the $\{O_i, \boldsymbol{x}_i, \boldsymbol{y}_i, \boldsymbol{z}_i\}$ frame and in the undeformed configuration
$\boldsymbol{S}_i \in \mathbb{R}^{3\times M_i}$	Small displacement shape function matrix
$\dot{\boldsymbol{v}}_i \in \mathbb{R}^3$	Linear acceleration of the origin O_i of the ith frame with respect to the origin of the world frame expressed in the world frame
$\boldsymbol{\omega}_i, \dot{\boldsymbol{\omega}}_i \in \mathbb{R}^3$	Angular velocity and acceleration of the local FFR attached to link i expressed in the world frame
$\dot{\boldsymbol{v}}'_{i+1} \in \mathbb{R}^3$	Component of the linear acceleration of the origin O_i of the ith frame dependent on the angular velocity of the local FFR attached to link i
$\boldsymbol{g}$	Gravity acceleration in the world frame
$\hat{\boldsymbol{A}}_i \in \mathbb{R}^{3\times 3}$	Rotation matrix defining *small* rotations of the frame $\{O'_i, \boldsymbol{x}'_i, \boldsymbol{y}'_i, \boldsymbol{z}'_i\}$ with respect to the FFR attached to link i
$\hat{\boldsymbol{S}}_i \in \mathbb{R}^{3\times M_i}$	Small rotation shape function matrix
$\bar{\boldsymbol{A}}_i \in \mathbb{R}^{3\times 3}$	Rotation matrix defining a rotation of the frame $\{O_{i+1}, \boldsymbol{x}_{i+1}, \boldsymbol{y}_{i+1}, \boldsymbol{z}_{i+1}\}$ of an angle θ_i about an axis defined in the frame $\{O'_i, \boldsymbol{x}'_i, \boldsymbol{y}'_i, \boldsymbol{z}'_i\}$ by the constant unit vector $\hat{\boldsymbol{z}}'_i$
$\dot{\boldsymbol{\omega}}'_{i+1} \in \mathbb{R}^3$	Component of the angular acceleration of the local FFR attached to link i dependent on the angular velocity of the frame i
$\dot{\boldsymbol{V}}_i = \begin{bmatrix} \dot{\boldsymbol{\omega}}_i \\ \dot{\boldsymbol{v}}_i \end{bmatrix} \in \mathbb{R}^6$	Spatial acceleration of the local FFR attached to link i
$\dot{\boldsymbol{V}}'_i = \begin{bmatrix} \dot{\boldsymbol{\omega}}'_i \\ \dot{\boldsymbol{v}}'_i \end{bmatrix} \in \mathbb{R}^6$	Component of the spatial acceleration of the local FFR attached to link i dependent on the angular velocity of the frame $i-1$
$\boldsymbol{P}_{i,j}$	Matrix to shift reference point from O_j to O_i
$\boldsymbol{P}_i$	Shorthand for $\boldsymbol{P}_{i+1,i}$
$\boldsymbol{B}_{\theta,i} \in \mathbb{R}^6$	Rotation axes in spatial vector notation
$\boldsymbol{B}_{q,i} \in \mathbb{R}^{6\times M_i}$	Shape function matrices in spatial vector notation
$\boldsymbol{\mathcal{P}} \in \mathbb{R}^{6N\times 6N}$	Global matrix to shift reference points
$\dot{\boldsymbol{\mathcal{V}}} = \text{col}\{\dot{\boldsymbol{V}}_i\} \in \mathbb{R}^{6N}$	Global vector of spatial accelerations
$\boldsymbol{\mathcal{B}}_\theta$	Global matrix of rotation axes in spatial vector notation
$\boldsymbol{\mathcal{B}}_q$	Global matrix of shape function matrices in spatial vector notation
$I_i^1 = m_i$	Mass of link i
$\mathbf{I}_i^2 = m_i \bar{\boldsymbol{r}}_i, \mathbf{I}_{j,i}^3 \in \mathbb{R}^3$	Inertia invariants of link i, with $\bar{\boldsymbol{r}}_i$ being the position of the center of mass of link i in the undeformed configuration
$\mathbf{I}_i^4, \mathbf{I}_{j,i}^5 \in \mathbb{R}^{3\times M_i}$	Inertia invariants of link i
$\mathbf{I}_i^6 = \boldsymbol{M}_{e,i} \in \mathbb{R}^{M_i\times M_i}$	Structural mass matrix of link i
$\mathbf{I}_i^7 = \bar{\boldsymbol{I}}_i, \mathbf{I}_{j,i}^8, \mathbf{I}_{jk,i}^9 \in \mathbb{R}^{3\times 3}$	Inertia invariants of link i, with $\bar{\boldsymbol{I}}_i$ being the inertia tensor of link i in the undeformed configuration
$\mathbf{I}_{jk,i}^{10}, \mathbf{I}_{jk,i}^{11} \in \mathbb{R}^{M_i}$	Inertia invariants of link i
$m_i \tilde{\tilde{\boldsymbol{d}}}_{C,i}, \bar{\boldsymbol{J}}_i \in \mathbb{R}^{3\times 3}$	Terms of the ith link inertia matrix
$\bar{\boldsymbol{C}}_{t,i}^T, \bar{\boldsymbol{C}}_{r,i}^T \in \mathbb{R}^{3\times M_i}$	Terms of the ith link inertia matrix
$\boldsymbol{D}_{e,i}, \boldsymbol{K}_{e,i} \in \mathbb{R}^{M_i\times M_i}$	Structural damping and stiffness matrix of link i
$\boldsymbol{h}_{\omega,i}^r, \boldsymbol{h}_{\omega,i}^\theta \in \mathbb{R}^3, \boldsymbol{h}_{\omega,i}^f \in \mathbb{R}^{M_i}$	Vectors of gyroscopic and centripetal terms acting on link i
$\boldsymbol{h}_{e,i}^r, \boldsymbol{h}_{e,i}^\theta \in \mathbb{R}^3, \boldsymbol{h}_{e,i}^f \in \mathbb{R}^{M_i}$	Vectors of external forces applied at the body connectors of link i
$\boldsymbol{f}_i, \boldsymbol{n}_i \in \mathbb{R}^3$	Force and torque applied from link $i-1$ to link i at O_i
$\boldsymbol{F}_i = \begin{bmatrix} \boldsymbol{f}_i \\ \boldsymbol{n}_i \end{bmatrix} \in \mathbb{R}^6$	Spatial force applied from link $i-1$ to link i at O_i
$\boldsymbol{\mathcal{F}} = \text{col}\{\boldsymbol{F}_i\} \in \mathbb{R}^{6N}$	Global vector of interlink spatial forces
$\boldsymbol{I}_{vv,i} \in \mathbb{R}^{6\times 6}$	Partition of the ith link inertia matrix
$\boldsymbol{I}_{vq,i} \in \mathbb{R}^{6\times M_i}$	Partition of the ith link inertia matrix

https://doi.org/10.1017/S0263574715000934 Published online by Cambridge University Press

$\boldsymbol{C}_{v,i} \in \mathbb{R}^6$	Vector collecting gyroscopic and centripetal terms acting on link i
$\boldsymbol{\mathcal{I}}_{vv} = \text{diag}\{\boldsymbol{I}_{vv,i}\} \in \mathbb{R}^{6N\times 6N}$	Global matrix of partitions of link inertia matrices
$\boldsymbol{\mathcal{C}}_v = \text{col}\{\boldsymbol{C}_{v,i}\} \in \mathbb{R}^{6N}$	Global vector collecting gyroscopic and centripetal terms
$\boldsymbol{\mathcal{I}}_{vq} \in \mathbb{R}^{6N\times M}$	Global matrix of partitions of link inertia matrices
$\boldsymbol{\mathcal{M}}_e, \boldsymbol{\mathcal{K}}_e, \boldsymbol{\mathcal{D}}_e \in \mathbb{R}^{M\times M}$	Global matrices of structural mass, stiffness and damping of links
$\boldsymbol{\mathcal{C}}_f = \text{col}\{\boldsymbol{h}^f_{\omega,i}\} \in \mathbb{R}^M$	Global vector collecting gyroscopic and centripetal terms

1. Introduction

The increasing need of higher speeds, loads and accuracy in robotics applications requires the adoption of increasingly complex dynamic models, accounting for link flexibility in order to predict the dynamic behavior of robots and, above all, for control systems design. This is even more important in space robotics, where the adoption of lightweight robots, capable of moving heavy loads, is an essential design requirement.[1,2] Moreover, accounting for flexibility is also important in the field of humanoid robots.[3]

Deriving the dynamic model of a flexible manipulator, in such a way that it is suitable for real-time, model-based estimation and control strategies, is however a complex task, which has been mainly carried out according to the following conceptual scheme:

- A FFR is attached to each link and the positions of its points are described as the superposition of an undeformed component, defined with respect to an inertial frame, and a local flexible deformation, defined with respect to the FFR;
- Assuming small deformations and a linear theory of elasticity, the flexible deformation is represented by a finite linear combination of space dependent shape functions multiplying time dependent modal coordinates;
- The kinetic and potential energy of the manipulator, the latter split into elastic and gravitational, is first computed by recursively propagating the kinematic information from the base to the hand tip, as a function of the joint and modal coordinates and velocities, then the Lagrange–Euler formulation is applied to derive the motion equations.

In the robotics literature, the most widely adopted definition of the shape functions is the Assumed Modes Model (AMM),[4–10] where the shape functions are defined over the entire extension of the link and generally belong to the class of trigonometric functions, but some examples are also reported adopting the Finite Element Model (FEM),[11–13] where the shape functions are defined over small subdomains of the link, as polynomial functions. A thorough comparison of the two approaches has been reported by Theodore and Ghosal in ref. [14]. In particular, they recommend the AMM formulation for discretization of manipulator links with uniform cross-sectional geometries and single-link manipulators, whereas the finite elements (FE) formulation is recommended for complex cross-sectional geometries and for multilink manipulators. It must be pointed out that AMM is usually adopted in the case of simple geometries where global shape functions can be analytically computed, while FEM formulation is usually not feasible for any real-time or control application, as the cardinality of the state variables dramatically increases in the case of complex geometries

In the case of uniform mass density and time-independent mode shapes, the particular formulation of the shape functions does not necessarily enter in the motion equations of the manipulator. In fact, once suitable boundary conditions have been imposed (see in particular refs. [5, 14] for the AMM and ref. [15] for the FEM), and the shape functions have been completely defined, they need to be evaluated at the tip of the links only, while the spatial dependence is resolved by integration over the spatial domain of the links, introducing a number of constant parameters characterizing the mechanical properties.

In turn, solid modeling packages for FEA can be conveniently used for the off-line computation of the above-mentioned parameters, particularly in the case of complex geometries, performing also an orthonormalization of mode shapes,[16] which is of great importance for model simplification. Without using such tools, the analysis is almost always limited to the adoption of the

https://doi.org/10.1017/S0263574715000934 Published online by Cambridge University Press

Euler–Bernoulli beam model for the flexible links,[4,6,8,11,13,14] applied to planar[5,7,12] or even single link manipulators.[9,17]

The Lagrange–Euler formulation results in a symbolic, closed form, dynamic model of the manipulator, and it is best suited for study of dynamic properties and analysis of control schemes. On the other hand, for implementation of real-time, model-based control schemes, the Newton–Euler formulation is generally preferred,[18] because of its computational efficiency. It must be anyway pointed out that some Lagrange–Euler formulations have been proposed, in particular recursive formulations,[4,19,20] which are as efficient as the Newton–Euler one.

On the contrary of the Lagrange–Euler formulation, where the dynamic model of the manipulator is obtained as a whole, in the Newton–Euler formulation the motion equations are outlined separately for each (floating) link, and the forward propagation of the kinematic quantities, common to the Lagrange–Euler approach, is followed by a backward propagation of forces/torques from the tip to the base, and by a projection of the joint constraint forces on the axes of motion. This computational procedure is usually carried out by means of recursive algorithms, while in this paper an explicit model is provided.

The Newton–Euler formulation is usually adopted in multibody system dynamic analysis, where components representing the objects are connected in order to form complex mechanisms. In this context the Newton–Euler formulation is more suitable to a modular approach with respect to the Lagrangian formulation, where the equations of motion of the mechanism are obtained as a whole. The FFR approach is also the most widely adopted(1). In particular, multibody dynamics methods have been applied to model flexible manipulators in refs. [24–29].

The AMM is also widely adopted in flexible multibody dynamics, together with the use of FE computer codes as preprocessors. In fact, most commercial FEA packages[30–32] can reduce the huge number of nodal coordinates to a much smaller number of modal coordinates (two or three in the case of robotic manipulators, according to ref. [14]). This task is usually carried out by means of the classical Craig–Bampton method[33] or other recently proposed methods,[34–37] and the flexible body parameters needed for flexible multibody simulation are stored either in ASCII or binary files after the analysis.

In this paper, a dynamic model of flexible manipulators, based on the Newton–Euler approach and on the adoption of the spatial vector notation,[38–40] is developed(2). The model is obtained in closed form with respect to the joint angles and the global vector of elastic coordinates, furthermore the inertia matrix and the nonlinear quadratic velocity terms are explicitly computed in the same context. All the model input data can be analytically computed according to either AMM or FEM formulation (an example in the case of the FEM of a beam is reported in ref. [44]) or, in the case of complex geometries and/or deformation fields, directly acquired as the output of most commercial FEM packages.

The closed form Newton–Euler dynamic model of flexible manipulators is then validated by comparing a simulation obtained with a Matlab implementation against the multibody approach in a classical example often proposed in literature. A further simulation is carried out in order to compare the model against experimental results provided by the MERIt dataset. The MERIt project,[45] developed by the Technisce Universität Dortmund, which the authors would primarily like to thank, makes freely available a set of measurement data carried out by the TUDOR experimental flexible robot.

Notwithstanding the original aim of MERIt is the identification of manipulator's dynamics, in the context of this work a subset of the experiments provided by the dataset has been reproduced by means of the Matlab/Simulink simulation environment, and results have been compared with the measurements, with the aim of validating the closed form model.

(1)In the case of large deformation problems, a different but equivalent approach is also adopted, the absolute nodal coordinate formulation (ANCF).[21–23] The ANCF, adopting absolute displacements and global slopes as nodal coordinates, results in a body constant mass matrix, zero centrifugal and Coriolis inertia forces, and highly nonlinear elastic terms, even in the case of linear elastic behavior.

(2)A similar approach has been also adopted in ref. [41], while in ref. [42] a recursive formulation is obtained, in which the Newton–Euler motion equations are derived for links and joints in terms of position and orientation of the FFR. In ref. [43] a $O(n)$ mass matrix inversion method using Lie derivatives has been also proposed.

https://doi.org/10.1017/S0263574715000934 Published online by Cambridge University Press

Table I. Link data.

M_i	Number of modal coordinates
$I_i^1, \boldsymbol{I}_i^2, \boldsymbol{I}_{j,i}^3, \boldsymbol{I}_i^4, \boldsymbol{I}_{j,i}^5, \boldsymbol{I}_i^6, \boldsymbol{I}_i^7, \boldsymbol{I}_{j,i}^8, \boldsymbol{I}_{jk,i}^9$	Inertia invariants
$\boldsymbol{K}_{e,i}$	Structural stiffness matrix
$\boldsymbol{S}_i, \hat{\boldsymbol{S}}_i$	Shape functions matrices
$\bar{\boldsymbol{u}}_{0i}$	Undeformed relative position between FFRs
$\hat{\boldsymbol{z}}'_{i-1}$	Joint rotation axis

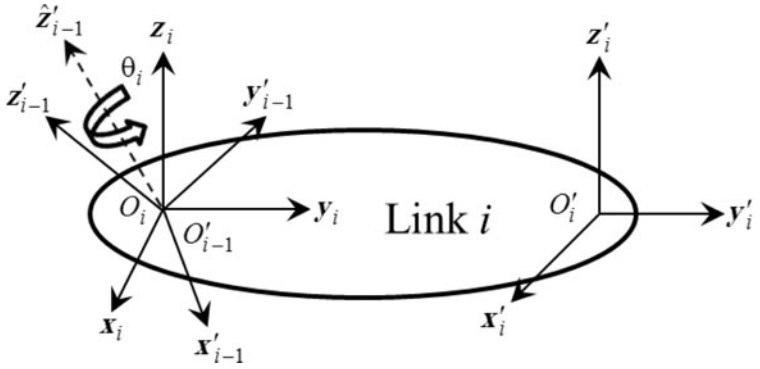


Fig. 1. Reference frames.

The paper is organized as follows: Section 2 describes the closed-form model, Section 3.1 reports the simulation results of the benchmark, while the comparison against experimental results is carried out in Section 3.2. Section 4 concludes the paper.

2. Closed form Newton–Euler Dynamic Model of Flexible Manipulators

The dynamic model of the flexible manipulator will be derived in the following closed form:

$$\boldsymbol{\mathcal{M}}_{\theta\theta}(\boldsymbol{\theta}, \boldsymbol{q})\ddot{\boldsymbol{\theta}} + \boldsymbol{\mathcal{M}}_{\theta q}(\boldsymbol{\theta}, \boldsymbol{q})\ddot{\boldsymbol{q}} + \boldsymbol{\mathcal{C}}_{\theta}(\boldsymbol{\theta}, \boldsymbol{q}, \dot{\boldsymbol{\theta}}, \dot{\boldsymbol{q}}) = \boldsymbol{\tau}, \tag{1}$$

$$\boldsymbol{\mathcal{M}}_{\theta q}^T(\boldsymbol{\theta}, \boldsymbol{q})\ddot{\boldsymbol{\theta}} + \boldsymbol{\mathcal{M}}_{qq}(\boldsymbol{\theta}, \boldsymbol{q})\ddot{\boldsymbol{q}} + \boldsymbol{\mathcal{D}}_e\dot{\boldsymbol{q}} + \boldsymbol{\mathcal{K}}_e\boldsymbol{q} + \boldsymbol{\mathcal{C}}_{\boldsymbol{q}}(\boldsymbol{\theta}, \boldsymbol{q}, \dot{\boldsymbol{\theta}}, \dot{\boldsymbol{q}}) = \boldsymbol{0}, \tag{2}$$

where $\boldsymbol{\theta} = \text{col}\{\theta_i\} \in \mathbb{R}^N, \boldsymbol{q} = \text{col}\{\boldsymbol{q}_i\} \in \mathbb{R}^M, \boldsymbol{\tau} = \text{col}\{\tau_i\} \in \mathbb{R}^N$, and $\theta_i, \boldsymbol{q}_i, \tau_i$, are the joint angles, the M_i-dimensional vector of modal coordinates of link i and the joint torques respectively. Furthermore $M = \sum_{i=1}^N M_i$. Thus, all matrices and vectors in Eqs. (1), (2) will be directly computed starting from link data, summarized in Table I.

2.1. Kinematics

For the sake of simplicity, a flexible manipulator connected by only revolute joints is considered, anyway the model can be easily modified to account for prismatic joints. Let the local FFR attached to link i be $\{O_i, \boldsymbol{x}_i, \boldsymbol{y}_i, \boldsymbol{z}_i\}$ (Fig. 1), and let $\{O'_i, \boldsymbol{x}'_i, \boldsymbol{y}'_i, \boldsymbol{z}'_i\}$ be another local reference frame, having the same orientation of the FFR frame in the undeformed configuration and with the origin O'_i coinciding with the origin O_{i+1} of the FFR of the next link in the chain. The angle θ_i is the coordinate of the joint connecting link i to link $i-1$, while $\hat{\boldsymbol{z}}'_{i-1}$ is the axis of rotation in the frame $\{O'_{i-1}, \boldsymbol{x}'_{i-1}, \boldsymbol{y}'_{i-1}, \boldsymbol{z}'_{i-1}\}$.

Remark 1. The notation adopted to describe the undeformed configuration is redundant with respect to the notations usually adopted in robotics, i.e., the Denavit–Hartenberg notation.[46] However, it is compliant with the description of bodies in FEM packages, which is necessary to describe distributed flexibility in case of complex geometries of links.

If small elastic deflections are considered, the infinite dimensional deformation field on the body can be approximated by a functional basis space with finite dimension, say M_i, so that the position

https://doi.org/10.1017/S0263574715000934 Published online by Cambridge University Press

$\boldsymbol{p}_{i+1}$ of the origin O_{i+1} of the $(i+1)$th frame with respect to the world reference frame is given by:

$$\boldsymbol{p}_{i+1} = \boldsymbol{p}_i + \boldsymbol{p}_{i+1,i}, \tag{3}$$

$$\boldsymbol{p}_{i+1,i} = \boldsymbol{A}_i \bar{\boldsymbol{u}}_i = \boldsymbol{A}_i \bar{\boldsymbol{u}}_{0,i} + \boldsymbol{A}_i \boldsymbol{S}_i \boldsymbol{q}_i, \tag{4}$$

where $\boldsymbol{A}_i$ is the (3×3) rotation matrix relating the FFR and the world reference frame, $\bar{\boldsymbol{u}}_{0,i}$ is the position vector relating the two frames in the undeformed configuration[3], $\boldsymbol{S}_i$ is the $[3 \times M_i]$ shape function matrix (i.e., a matrix of functions defined over the body domain and used as a basis to describe the deformation field of the body itself) and $\boldsymbol{q}_i$ is the M_i-dimensional vector of modal coordinates. Accordingly, the relation between the linear accelerations of the two frames, for $i = 1, \ldots, (N-1)$, is given by:

$$\dot{\boldsymbol{v}}_{i+1} = \dot{\boldsymbol{v}}_i - \tilde{\boldsymbol{p}}_{i+1,i} \dot{\boldsymbol{\omega}}_i + \boldsymbol{A}_i \boldsymbol{S}_i \ddot{\boldsymbol{q}}_i + \dot{\boldsymbol{v}}'_{i+1}, \tag{5}$$

$$\dot{\boldsymbol{v}}'_{i+1} = \boldsymbol{\omega}_i \times \left(\boldsymbol{\omega}_i \times \boldsymbol{p}_{i+1,i} + \boldsymbol{A}_i \boldsymbol{S}_i \dot{\boldsymbol{q}}_i \right), \tag{6}$$

where $\tilde{\boldsymbol{p}}$ is the skew-symmetric matrix associated to vector $\boldsymbol{p}$. For $i = 0$, instead, it is:

$$\dot{\boldsymbol{v}}_1 = \dot{\boldsymbol{v}}'_1, \tag{7}$$

$$\dot{\boldsymbol{v}}'_1 = -\boldsymbol{g}, \tag{8}$$

where $\boldsymbol{g}$ is the gravity acceleration in the world frame. In this way it is possible to easily account for gravitational terms in the motion equations.

The rotation matrix $\boldsymbol{A}_{i+1}$ of the $(i+1)$th frame with respect to the world frame is in turn related to the rotation matrix $\boldsymbol{A}_i$ as follows:

$$\boldsymbol{A}_{i+1} = \boldsymbol{A}_i \hat{\boldsymbol{A}}_i \bar{\boldsymbol{A}}_i, \tag{9}$$

$$\hat{\boldsymbol{A}}_i = \boldsymbol{U} + \widetilde{\left(\hat{\boldsymbol{S}}_i \boldsymbol{q}_i \right)}, \tag{10}$$

$$\bar{\boldsymbol{A}}_i = \bar{\boldsymbol{A}}_i (\hat{\boldsymbol{z}}'_i, \theta_{i+1}), \tag{11}$$

where $\boldsymbol{U}$ is the 3×3 identity matrix, and matrix $\hat{\boldsymbol{A}}_i$ defines *small* rotations of the frame $\{O'_i, \boldsymbol{x}'_i, \boldsymbol{y}'_i, \boldsymbol{z}'_i\}$ with respect to the FFR due to body deformation, obtained by a modal superposition through the $[3 \times M_i]$ shape function matrix $\hat{\boldsymbol{S}}_i$, while matrix $\bar{\boldsymbol{A}}_i$ defines a rotation of the frame $\{O_{i+1}, \boldsymbol{x}_{i+1}, \boldsymbol{y}_{i+1}, \boldsymbol{z}_{i+1}\}$ of an angle θ_{i+1} about an axis defined in the frame $\{O'_i, \boldsymbol{x}'_i, \boldsymbol{y}'_i, \boldsymbol{z}'_i\}$ by the constant unit vector $\hat{\boldsymbol{z}}'_i$.

The angular velocity and acceleration of the $(i+1)$th frame, for $i = 1, \ldots, (N-1)$, are therefore given by:

$$\boldsymbol{\omega}_{i+1} = \boldsymbol{\omega}_i + \boldsymbol{A}_i \hat{\boldsymbol{S}}_i \dot{\boldsymbol{q}}_i + \boldsymbol{A}_i \hat{\boldsymbol{A}}_i \hat{\boldsymbol{z}}'_i \dot{\theta}_{i+1}, \tag{12}$$

$$\dot{\boldsymbol{\omega}}_{i+1} = \dot{\boldsymbol{\omega}}_i + \boldsymbol{A}_i \hat{\boldsymbol{A}}_i \hat{\boldsymbol{z}}'_i \ddot{\theta}_{i+1} + \boldsymbol{A}_i \hat{\boldsymbol{S}}_i \ddot{\boldsymbol{q}}_i + \dot{\boldsymbol{\omega}}'_{i+1}, \tag{13}$$

$$\dot{\boldsymbol{\omega}}'_{i+1} = \boldsymbol{\omega}_i \times \left(\boldsymbol{A}_i \hat{\boldsymbol{S}}_i \dot{\boldsymbol{q}}_i + \boldsymbol{A}_i \hat{\boldsymbol{A}}_i \hat{\boldsymbol{z}}'_i \dot{\theta}_{i+1} \right) + \boldsymbol{A}_i \widetilde{\left(\hat{\boldsymbol{S}}_i \dot{\boldsymbol{q}}_i \right)} \hat{\boldsymbol{z}}'_i \dot{\theta}_{i+1}, \tag{14}$$

while for $i = 0$,

$$\boldsymbol{\omega}_1 = \boldsymbol{A}_0 \hat{\boldsymbol{A}}_0 \hat{\boldsymbol{z}}'_0 \dot{\theta}_1 \quad (\boldsymbol{A}_0 = \hat{\boldsymbol{A}}_0 = \boldsymbol{U}), \tag{15}$$

$$\dot{\boldsymbol{\omega}}_1 = \boldsymbol{A}_0 \hat{\boldsymbol{A}}_0 \hat{\boldsymbol{z}}'_0 \ddot{\theta}_1 + \dot{\boldsymbol{\omega}}'_1, \tag{16}$$

$$\dot{\boldsymbol{\omega}}'_1 = \boldsymbol{0}. \tag{17}$$

[3]The bar above a vector indicates that the vector is expressed with reference to the local FFR.

https://doi.org/10.1017/S0263574715000934 Published online by Cambridge University Press

Adopting the spatial vector notation,[38–40] thus defining

$$\dot{\boldsymbol{V}}_i = \begin{bmatrix} \dot{\boldsymbol{\omega}}_i, \\ \dot{\boldsymbol{v}}_i \end{bmatrix} \in \mathbb{R}^6, \quad \dot{\boldsymbol{V}}_i' = \begin{bmatrix} \dot{\boldsymbol{\omega}}_i' \\ \dot{\boldsymbol{v}}_i' \end{bmatrix} \in \mathbb{R}^6, \quad \boldsymbol{P}_i = \begin{bmatrix} \boldsymbol{U} & \boldsymbol{0} \\ -\tilde{\boldsymbol{p}}_{i+1,i} & \boldsymbol{U} \end{bmatrix} \in \mathbb{R}^{6\times 6}, \tag{18}$$

$$\boldsymbol{B}_{\theta,i} = \begin{bmatrix} \boldsymbol{A}_i \hat{\boldsymbol{A}}_i \hat{\boldsymbol{z}}_i \\ \boldsymbol{0} \end{bmatrix} \in \mathbb{R}^6, \quad \boldsymbol{B}_{q,i} = \begin{bmatrix} \boldsymbol{A}_i \hat{\boldsymbol{S}}_i \\ \boldsymbol{A}_i \boldsymbol{S}_i \end{bmatrix} \in \mathbb{R}^{6\times M_i}, \tag{19}$$

Equations (5) and (13) can be collected into:

$$\dot{\boldsymbol{V}}_i - \boldsymbol{P}_{i-1}\dot{\boldsymbol{V}}_{i-1} = \boldsymbol{B}_{\theta,i-1}\ddot{\theta}_i + \boldsymbol{B}_{q,i-1}\ddot{\boldsymbol{q}}_{i-1} + \dot{\boldsymbol{V}}_i'. \tag{20}$$

In turn, defining with N the number of the links, and with $M = \sum_{i=1}^{N} M_i$ the number of elastic variables, it is possible to collect all the Eq (20) into a single global equation of the form

$$\boldsymbol{\mathcal{P}}^T \dot{\boldsymbol{\mathcal{V}}} = \boldsymbol{\mathcal{B}}_\theta \ddot{\boldsymbol{\theta}} + \boldsymbol{\mathcal{B}}_q \ddot{\boldsymbol{q}} + \dot{\boldsymbol{\mathcal{V}}}', \tag{21}$$

with $\dot{\boldsymbol{\mathcal{V}}} = \text{col}\{\dot{\boldsymbol{V}}_i\} \in \mathbb{R}^{6N}$, $\dot{\boldsymbol{\mathcal{V}}}' = \text{col}\{\dot{\boldsymbol{V}}_i'\} \in \mathbb{R}^{6N}$

$$\boldsymbol{\mathcal{P}} = \begin{bmatrix} \boldsymbol{U} & -\boldsymbol{P}_1^T & \boldsymbol{0} & \dots & \boldsymbol{0} & \boldsymbol{0} \\ \boldsymbol{0} & \boldsymbol{U} & -\boldsymbol{P}_2^T & \dots & \boldsymbol{0} & \boldsymbol{0} \\ \boldsymbol{0} & \boldsymbol{0} & \boldsymbol{U} & \dots & \boldsymbol{0} & \boldsymbol{0} \\ \vdots & \vdots & \vdots & \ddots & \vdots & \vdots \\ \boldsymbol{0} & \boldsymbol{0} & \boldsymbol{0} & \dots & \boldsymbol{U} & -\boldsymbol{P}_{N-1}^T \\ \boldsymbol{0} & \boldsymbol{0} & \boldsymbol{0} & \dots & \boldsymbol{0} & \boldsymbol{U} \end{bmatrix} \in \mathbb{R}^{6N\times 6N}, \tag{22}$$

$$\boldsymbol{\mathcal{B}}_\theta = \begin{bmatrix} \boldsymbol{B}_{\theta,0} & \boldsymbol{0} & \boldsymbol{0} & \dots & \boldsymbol{0} & \boldsymbol{0} \\ \boldsymbol{0} & \boldsymbol{B}_{\theta,1} & \boldsymbol{0} & \dots & \boldsymbol{0} & \boldsymbol{0} \\ \boldsymbol{0} & \boldsymbol{0} & \boldsymbol{B}_{\theta,2} & \dots & \boldsymbol{0} & \boldsymbol{0} \\ \vdots & \vdots & \vdots & \ddots & \vdots & \vdots \\ \boldsymbol{0} & \boldsymbol{0} & \boldsymbol{0} & \dots & \boldsymbol{B}_{\theta,N-2} & \boldsymbol{0} \\ \boldsymbol{0} & \boldsymbol{0} & \boldsymbol{0} & \dots & \boldsymbol{0} & \boldsymbol{B}_{\theta,N-1} \end{bmatrix} \in \mathbb{R}^{6N\times N}, \tag{23}$$

$$\boldsymbol{\mathcal{B}}_q = \begin{bmatrix} \boldsymbol{0} & \boldsymbol{0} & \boldsymbol{0} & \dots & \boldsymbol{0} & \boldsymbol{0} \\ \boldsymbol{B}_{q,1} & \boldsymbol{0} & \boldsymbol{0} & \dots & \boldsymbol{0} & \boldsymbol{0} \\ \boldsymbol{0} & \boldsymbol{B}_{q,2} & \boldsymbol{0} & \dots & \boldsymbol{0} & \boldsymbol{0} \\ \vdots & \vdots & \vdots & \ddots & \vdots & \vdots \\ \boldsymbol{0} & \boldsymbol{0} & \boldsymbol{0} & \dots & \boldsymbol{0} & \boldsymbol{0} \\ \boldsymbol{0} & \boldsymbol{0} & \boldsymbol{0} & \dots & \boldsymbol{B}_{q,N-1} & \boldsymbol{0} \end{bmatrix} \in \mathbb{R}^{6N\times M}. \tag{24}$$

https://doi.org/10.1017/S0263574715000934 Published online by Cambridge University Press

2.2. Dynamics

The motion equations for the ith flexible link, expressed in the FFR, can be developed by applying the principle of virtual work,[44,47–50] yielding

$$\begin{bmatrix} m_i \boldsymbol{U} & m_i \tilde{\tilde{\boldsymbol{d}}}_{C,i}^T & \bar{\boldsymbol{C}}_{t,i}^T \\ m_i \tilde{\tilde{\boldsymbol{d}}}_{C,i} & \bar{\boldsymbol{J}}_i & \bar{\boldsymbol{C}}_{r,i}^T \\ \bar{\boldsymbol{C}}_{t,i} & \bar{\boldsymbol{C}}_{r,i} & \boldsymbol{M}_{e,i} \end{bmatrix} \begin{bmatrix} \dot{\bar{\boldsymbol{v}}}_i \\ \dot{\bar{\boldsymbol{\omega}}}_i \\ \ddot{\boldsymbol{q}}_i \end{bmatrix} = \begin{bmatrix} \boldsymbol{0}_3 \\ \boldsymbol{0}_3 \\ -\boldsymbol{K}_{e,i}\boldsymbol{q}_i - \boldsymbol{D}_{e,i}\dot{\boldsymbol{q}}_i \end{bmatrix} + \begin{bmatrix} \boldsymbol{h}_{\omega,i}^r \\ \boldsymbol{h}_{\omega,i}^\theta \\ \boldsymbol{h}_{\omega,i}^f \end{bmatrix} + \begin{bmatrix} \boldsymbol{h}_{e,i}^r \\ \boldsymbol{h}_{e,i}^\theta \\ \boldsymbol{h}_{e,i}^f \end{bmatrix} \tag{25}$$

where $\boldsymbol{M}_{e,i} \in \mathbb{R}^{M_i \times M_i}$, $\boldsymbol{D}_{e,i} \in \mathbb{R}^{M_i \times M_i}$, $\boldsymbol{K}_{e,i} \in \mathbb{R}^{M_i \times M_i}$ are the structural mass, damping and stiffness matrix, respectively. Regarding the flexible degrees of freedom (DOFs), $\boldsymbol{h}_{\omega,i}^r \in \mathbb{R}^3$, $\boldsymbol{h}_{\omega,i}^\theta \in \mathbb{R}^3$, $\boldsymbol{h}_{\omega,i}^f \in \mathbb{R}^{M_i}$ are the vectors of gyroscopic and centripetal terms, and $\boldsymbol{h}_{e,i}^r \in \mathbb{R}^3$, $\boldsymbol{h}_{e,i}^\theta \in \mathbb{R}^3$, $\boldsymbol{h}_{e,i}^f \in \mathbb{R}^{M_i}$ are the vectors of external forces, applied at the body connectors.

The terms in the generalized mass matrix depend on nine inertia invariants (see Appendix A), which in turn depend on the shape functions and on the body mass distribution:

$$m_i = I_i^1 \in \mathbb{R}, \tag{26}$$

$$m_i \tilde{\tilde{\boldsymbol{d}}}_{C,i} = \left(\tilde{\boldsymbol{I}}_i^2 + \sum_{j=1}^{M_i} \tilde{\boldsymbol{I}}_{j,i}^3 q_{j,i} \right) \in \mathbb{R}^{3\times 3}, \tag{27}$$

$$\bar{\boldsymbol{C}}_{t,i}^T = \begin{bmatrix} \boldsymbol{I}_{1,i}^3 & \boldsymbol{I}_{2,i}^3 & \dots & \boldsymbol{I}_{M,i}^3 \end{bmatrix} \in \mathbb{R}^{3\times M_i}, \tag{28}$$

$$\bar{\boldsymbol{C}}_{r,i}^T = \left(\boldsymbol{I}_i^4 + \sum_{j=1}^{M_i} \boldsymbol{I}_{j,i}^5 q_{j,i} \right) \in \mathbb{R}^{3\times M_i}, \tag{29}$$

$$\boldsymbol{M}_{e,i} = \boldsymbol{I}_i^6 \in \mathbb{R}^{M_i \times M_i}, \tag{30}$$

$$\bar{\boldsymbol{J}}_i = \left(\boldsymbol{I}_i^7 - \sum_{j=1}^{M_i} \left(\boldsymbol{I}_{j,i}^{8T} + \boldsymbol{I}_{j,i}^8 \right) q_{j,i} - \sum_{j=1}^{M_i} \sum_{k=1}^{M_i} \boldsymbol{I}_{jk,i}^9 q_{j,i} q_{k,i} \right) \in \mathbb{R}^{3\times 3}. \tag{31}$$

The vectors of gyroscopic and centripetal terms relevant to the rigid DOFs are given by

$$\boldsymbol{h}_{\omega,i}^r = -\bar{\boldsymbol{\omega}}_i \times \left(\bar{\boldsymbol{\omega}}_i \times m_i \bar{\boldsymbol{d}}_{C,i} + 2\bar{\boldsymbol{C}}_{t,i}^T \dot{\boldsymbol{q}}_i \right), \tag{32}$$

$$\boldsymbol{h}_{\omega,i}^\theta = -\bar{\boldsymbol{\omega}}_i \times \left(\bar{\boldsymbol{J}}_i \bar{\boldsymbol{\omega}}_i + \bar{\boldsymbol{C}}_{r,i}^T \dot{\boldsymbol{q}}_i \right) - \dot{\bar{\boldsymbol{J}}}_i \bar{\boldsymbol{\omega}}_i, \tag{33}$$

where

$$\dot{\bar{\boldsymbol{J}}}_i = -\sum_{j=1}^{M_i} \left(\boldsymbol{I}_{j,i}^{8T} + \boldsymbol{I}_{j,i}^8 \right) \dot{q}_{j,i} - \sum_{j=1}^{M_i} \sum_{k=1}^{M_i} \boldsymbol{I}_{jk,i}^9 (\dot{q}_{j,i} q_{k,i} + q_{j,i} \dot{q}_{k,i}). \tag{34}$$

The computation of the vector $\boldsymbol{h}_{\omega,i}^f$ relevant to the elastic DOFs, instead, is much more involved and requires the definition of two more inertia invariants, namely $\boldsymbol{I}_{jk,i}^{10}$ and $\boldsymbol{I}_{jk,i}^{11}$, which however can be computed from invariants $\boldsymbol{I}_{j,i}^8$ and $\boldsymbol{I}_{jk,i}^9$ (Appendix A).

$$\begin{aligned} \boldsymbol{h}_{\omega,i}^f = & \begin{bmatrix} \bar{\omega}_{1,i} \left(\sum_{j=1}^3 \boldsymbol{d}_{jj,i} \right) - \bar{\boldsymbol{\omega}}_i^T \boldsymbol{D}_{1,i} \\ \bar{\omega}_{2,i} \left(\sum_{j=1}^3 \boldsymbol{d}_{jj,i} \right) - \bar{\boldsymbol{\omega}}_i^T \boldsymbol{D}_{2,i} \\ \bar{\omega}_{3,i} \left(\sum_{j=1}^3 \boldsymbol{d}_{jj,i} \right) - \bar{\boldsymbol{\omega}}_i^T \boldsymbol{D}_{3,i} \end{bmatrix}^T \bar{\boldsymbol{\omega}}_i \\ & - 2 \left[\bar{\omega}_{1,i} \left(\boldsymbol{I}_{32,i}^{11} - \boldsymbol{I}_{23,i}^{11} \right) + \bar{\omega}_{2,i} \left(\boldsymbol{I}_{13,i}^{11} - \boldsymbol{I}_{31,i}^{11} \right) + \bar{\omega}_{3,i} \left(\boldsymbol{I}_{21,i}^{11} - \boldsymbol{I}_{12,i}^{11} \right) \right] \dot{\boldsymbol{q}}_i, \end{aligned} \tag{35}$$

https://doi.org/10.1017/S0263574715000934 Published online by Cambridge University Press

where

$$\boldsymbol{D}_{j,i} = \begin{bmatrix} \boldsymbol{d}_{j1,i} \\ \boldsymbol{d}_{j2,i} \\ \boldsymbol{d}_{j3,i} \end{bmatrix} = \begin{bmatrix} \boldsymbol{I}^{10}_{j1,i} \\ \boldsymbol{I}^{10}_{j2,i} \\ \boldsymbol{I}^{10}_{j3,i} \end{bmatrix} + \begin{bmatrix} \boldsymbol{q}_i^T \boldsymbol{I}^{11}_{j1,i} \\ \boldsymbol{q}_i^T \boldsymbol{I}^{11}_{j2,i} \\ \boldsymbol{q}_i^T \boldsymbol{I}^{11}_{j3,i} \end{bmatrix} \qquad j = 1, 2, 3 \tag{36}$$

Matrix $\boldsymbol{D}_{e,i}$, modeling the dissipative properties of the material, could be defined as $\boldsymbol{D}_{e,i} = \alpha_i \boldsymbol{M}_{e,i} + \beta_i \boldsymbol{K}_{e,i}$, where α_i and β_i are the so-called Rayleigh damping coefficients.

Defining with $\boldsymbol{f}_i, \boldsymbol{n}_i$ the force and torque applied from link $i-1$ to link i at O_i, with reference to the world frame, the vectors of external forces are given by:

$$\boldsymbol{h}^r_{e,i} = \bar{\boldsymbol{f}}_i - \bar{\boldsymbol{f}}_{i+1}, \tag{37}$$

$$\boldsymbol{h}^\theta_{e,i} = \bar{\boldsymbol{n}}_i - \bar{\boldsymbol{n}}_{i+1} - \tilde{\bar{\boldsymbol{u}}}_i \bar{\boldsymbol{f}}_{i+1}, \tag{38}$$

$$\boldsymbol{h}^f_{e,i} = -\boldsymbol{S}_i^T \bar{\boldsymbol{f}}_{i+1} - \hat{\boldsymbol{S}}_i^T \bar{\boldsymbol{n}}_{i+1}, \tag{39}$$

Collecting the torque and force in a spatial vector $\boldsymbol{F}_i = [\,\boldsymbol{n}_i^T \;\; \boldsymbol{f}_i^T\,]^T \in \mathbb{R}^6$, and projecting the motion equations relevant to the angular and linear accelerations on the world frame one obtains

$$\boldsymbol{I}_{vv,i} \dot{\boldsymbol{V}}_i + \boldsymbol{I}_{vq,i} \ddot{\boldsymbol{q}}_i - \boldsymbol{C}_{v,i} = \boldsymbol{F}_i - \boldsymbol{P}_i^T \boldsymbol{F}_{i+1}, \tag{40}$$

where

$$\boldsymbol{I}_{vv,i} = \begin{bmatrix} \boldsymbol{A}_i \bar{\boldsymbol{J}}_i \boldsymbol{A}_i^T & m_i \boldsymbol{A}_i \tilde{\bar{\boldsymbol{d}}}_{C,i} \boldsymbol{A}_i^T \\ m_i \boldsymbol{A}_i \tilde{\bar{\boldsymbol{d}}}^T_{C,i} \boldsymbol{A}_i^T & m_i \boldsymbol{U} \end{bmatrix} \in \mathbb{R}^{6\times 6}, \tag{41}$$

$$\boldsymbol{I}_{vq,i} = \begin{bmatrix} \boldsymbol{A}_i \bar{\boldsymbol{C}}^T_{r,i} \\ \boldsymbol{A}_i \bar{\boldsymbol{C}}^T_{t,i} \end{bmatrix} \in \mathbb{R}^{6\times M_i}, \quad \boldsymbol{C}_{v,i} = \begin{bmatrix} \boldsymbol{A}_i \boldsymbol{h}^\theta_{\omega,i} \\ \boldsymbol{A}_i \boldsymbol{h}^r_{\omega,i} \end{bmatrix} \in \mathbb{R}^6, \tag{42}$$

A single global equation can be again obtained by defining $\boldsymbol{\mathcal{I}}_{vv} = \text{diag}\{\boldsymbol{I}_{vv,i}\} \in \mathbb{R}^{6N\times 6N}$, $\boldsymbol{\mathcal{F}} = \text{col}\{\boldsymbol{F}_i\} \in \mathbb{R}^{6N}$, $\boldsymbol{\mathcal{C}}_v = \text{col}\{\boldsymbol{C}_{v,i}\} \in \mathbb{R}^{6N}$ and

$$\boldsymbol{\mathcal{I}}_{vq} = \begin{bmatrix} \boldsymbol{I}_{vq,1} & \boldsymbol{0} & \boldsymbol{0} & \dots & \boldsymbol{0} & \boldsymbol{0} \\ \boldsymbol{0} & \boldsymbol{I}_{vq,2} & \boldsymbol{0} & \dots & \boldsymbol{0} & \boldsymbol{0} \\ \boldsymbol{0} & \boldsymbol{0} & \boldsymbol{I}_{vq,3} & \dots & \boldsymbol{0} & \boldsymbol{0} \\ \vdots & \vdots & \vdots & \ddots & \vdots & \vdots \\ \boldsymbol{0} & \boldsymbol{0} & \boldsymbol{0} & \dots & \boldsymbol{I}_{vq,N-1} & \boldsymbol{0} \\ \boldsymbol{0} & \boldsymbol{0} & \boldsymbol{0} & \dots & \boldsymbol{0} & \boldsymbol{I}_{vq,N} \end{bmatrix} \in \mathbb{R}^{6N\times M} \tag{43}$$

as follows:

$$\boldsymbol{\mathcal{I}}_{vv} \dot{\boldsymbol{\mathcal{V}}} + \boldsymbol{\mathcal{I}}_{vq} \ddot{\boldsymbol{q}} - \boldsymbol{\mathcal{C}}_v = \boldsymbol{\mathcal{P}} \boldsymbol{\mathcal{F}}. \tag{44}$$

A global equation can be also obtained for the dynamics of the elastic coordinates which, according to (25), are defined by:

$$\boldsymbol{I}^T_{vq,i} \dot{\boldsymbol{V}}_i + \boldsymbol{M}_{e,i} \ddot{\boldsymbol{q}}_i = -\boldsymbol{K}_{e,i} \boldsymbol{q}_i - \boldsymbol{D}_{e,i} \dot{\boldsymbol{q}}_i + \boldsymbol{h}^f_{\omega,i} - \boldsymbol{B}^T_{q,i} \boldsymbol{F}_{i+1}. \tag{45}$$

https://doi.org/10.1017/S0263574715000934 Published online by Cambridge University Press

Defining $\boldsymbol{\mathcal{M}}_e = \text{diag}\{\boldsymbol{M}_{e,i}\} \in \mathbb{R}^{M\times M}, \boldsymbol{\mathcal{K}}_e = \text{diag}\{\boldsymbol{K}_{e,i}\} \in \mathbb{R}^{M\times M}, \boldsymbol{\mathcal{D}}_e = \text{diag}\{\boldsymbol{D}_{e,i}\} \in \mathbb{R}^{M\times M}, \boldsymbol{\mathcal{C}}_f = \text{col}\{\boldsymbol{h}^f_{\omega,i}\} \in \mathbb{R}^M$ one obtains

$$\boldsymbol{\mathcal{I}}^T_{vq}\dot{\boldsymbol{\mathcal{V}}} + \boldsymbol{\mathcal{M}}_e\ddot{\boldsymbol{q}} + \boldsymbol{\mathcal{D}}_e\dot{\boldsymbol{q}} + \boldsymbol{\mathcal{K}}_e\boldsymbol{q} - \boldsymbol{\mathcal{C}}_f = -\boldsymbol{\mathcal{B}}^T_q\boldsymbol{\mathcal{F}} \tag{46}$$

2.3. Closed form model

By solving Eq. (21) with respect to $\dot{\boldsymbol{\mathcal{V}}}$, and Eq. (44) with respect to $\boldsymbol{\mathcal{F}}$, and substituting in Eq. (46) one obtains Eq. (2):

$$\boldsymbol{\mathcal{M}}^T_{\theta q}\ddot{\boldsymbol{\theta}} + \boldsymbol{\mathcal{M}}_{qq}\ddot{\boldsymbol{q}} + \boldsymbol{\mathcal{D}}_e\dot{\boldsymbol{q}} + \boldsymbol{\mathcal{K}}_e\boldsymbol{q} + \boldsymbol{\mathcal{C}}_{\boldsymbol{q}} = \boldsymbol{0} \tag{47}$$

where

$$\boldsymbol{\mathcal{M}}^T_{\theta q} = \left\{\left(\boldsymbol{\mathcal{I}}^T_{vq}\boldsymbol{\mathcal{P}}^{-T}\right) + \left[\boldsymbol{\mathcal{B}}^T_q\left(\boldsymbol{\mathcal{P}}^{-1}\boldsymbol{\mathcal{I}}_{vv}\boldsymbol{\mathcal{P}}^{-T}\right)\right]\right\}\boldsymbol{\mathcal{B}}_\theta, \tag{48}$$

$$\begin{aligned}\boldsymbol{\mathcal{M}}_{qq} = {} & \boldsymbol{\mathcal{M}}_e + \boldsymbol{\mathcal{B}}^T_q\left(\boldsymbol{\mathcal{P}}^{-1}\boldsymbol{\mathcal{I}}_{vv}\boldsymbol{\mathcal{P}}^{-T}\right)\boldsymbol{\mathcal{B}}_q \\ & + \left[\left(\boldsymbol{\mathcal{I}}^T_{vq}\boldsymbol{\mathcal{P}}^{-T}\right)\boldsymbol{\mathcal{B}}_q\right] + \left[\left(\boldsymbol{\mathcal{I}}^T_{vq}\boldsymbol{\mathcal{P}}^{-T}\right)\boldsymbol{\mathcal{B}}_q\right]^T,\end{aligned} \tag{49}$$

$$\begin{aligned}\boldsymbol{\mathcal{C}}_q = {} & \left\{\left(\boldsymbol{\mathcal{I}}^T_{vq}\boldsymbol{\mathcal{P}}^{-T}\right) + \left[\boldsymbol{\mathcal{B}}^T_q\left(\boldsymbol{\mathcal{P}}^{-1}\boldsymbol{\mathcal{I}}_{vv}\boldsymbol{\mathcal{P}}^{-T}\right)\right]\right\}\dot{\boldsymbol{\mathcal{V}}}' \\ & - \boldsymbol{\mathcal{B}}^T_q\left(\boldsymbol{\mathcal{P}}^{-1}\boldsymbol{\mathcal{C}}_v\right) - \boldsymbol{\mathcal{C}}_f.\end{aligned} \tag{50}$$

It must be recalled that matrix $\boldsymbol{\mathcal{P}}$ is invertible, and that its inverse is the upper-triangular matrix

$$\boldsymbol{\mathcal{P}}^{-1} = \begin{bmatrix} \boldsymbol{U} & \boldsymbol{P}^T_{2,1} & \boldsymbol{P}^T_{3,1} & \dots & \boldsymbol{P}^T_{N-1,1} & \boldsymbol{P}^T_{N,1} \\ \boldsymbol{0} & \boldsymbol{U} & \boldsymbol{P}^T_{3,2} & \dots & \boldsymbol{P}^T_{N-1,2} & \boldsymbol{P}^T_{N,2} \\ \boldsymbol{0} & \boldsymbol{0} & \boldsymbol{U} & \dots & \boldsymbol{P}^T_{N-1,3} & \boldsymbol{P}^T_{N,3} \\ \vdots & \vdots & \vdots & \ddots & \vdots & \vdots \\ \boldsymbol{0} & \boldsymbol{0} & \boldsymbol{0} & \dots & \boldsymbol{U} & \boldsymbol{P}^T_{N,N-1} \\ \boldsymbol{0} & \boldsymbol{0} & \boldsymbol{0} & \dots & \boldsymbol{0} & \boldsymbol{U} \end{bmatrix} \in \mathbb{R}^{6N\times 6N} \tag{51}$$

being

$$\boldsymbol{P}_i = \boldsymbol{P}_{i+1,i}, \quad \boldsymbol{P}_{i,k} = \boldsymbol{P}_{i,j}\boldsymbol{P}_{j,k}, \quad \boldsymbol{P}^{-1}_{i,j} = \boldsymbol{P}_{j,i}. \tag{52}$$

The joint input torque τ_i is equal to the scalar product between the ith joint rotation axis and the torque $\boldsymbol{n}_i$

$$\tau_i = \left(\boldsymbol{A}_{i-1}\hat{\boldsymbol{A}}_{i-1}\hat{\boldsymbol{z}}'_{i-1}\right)^T\boldsymbol{n}_i = \left[\left(\boldsymbol{A}_{i-1}\hat{\boldsymbol{A}}_{i-1}\hat{\boldsymbol{z}}'_{i-1}\right)^T \quad \boldsymbol{0}\right]\boldsymbol{F}_i = \boldsymbol{B}^T_{\theta,i-1}\boldsymbol{F}_i, \tag{53}$$

so that

$$\boldsymbol{\tau} = \boldsymbol{\mathcal{B}}^T_\theta\boldsymbol{\mathcal{F}} \tag{54}$$

from which Eq. (1) follows:

$$\boldsymbol{\mathcal{M}}_{\theta\theta}\ddot{\boldsymbol{\theta}} + \boldsymbol{\mathcal{M}}_{\theta q}\ddot{\boldsymbol{q}} + \boldsymbol{\mathcal{C}}_\theta = \boldsymbol{\tau} \tag{55}$$

where

$$\boldsymbol{\mathcal{M}}_{\theta\theta} = \left[\boldsymbol{\mathcal{B}}^T_\theta\left(\boldsymbol{\mathcal{P}}^{-1}\boldsymbol{\mathcal{I}}_{vv}\boldsymbol{\mathcal{P}}^{-T}\right)\right]\boldsymbol{\mathcal{B}}_\theta, \tag{56}$$

$$\boldsymbol{\mathcal{C}}_\theta = \left[\boldsymbol{\mathcal{B}}^T_\theta\left(\boldsymbol{\mathcal{P}}^{-1}\boldsymbol{\mathcal{I}}_{vv}\boldsymbol{\mathcal{P}}^{-T}\right)\right]\dot{\boldsymbol{\mathcal{V}}}' - \boldsymbol{\mathcal{B}}^T_\theta\left(\boldsymbol{\mathcal{P}}^{-1}\boldsymbol{\mathcal{C}}_v\right). \tag{57}$$

https://doi.org/10.1017/S0263574715000934 Published online by Cambridge University Press

Remark 2. Starting from matrices $\mathcal{I}_{vv}$ and $\mathcal{I}_{vq}$ the computation of the manipulator inertia matrix requires the computation of eight matrix products, namely:

$$\mathcal{M}_1 = \mathcal{P}^{-1}\mathcal{I}_{vv}\mathcal{P}^{-T}, \tag{58}$$

$$\mathcal{M}_2 = \mathcal{M}_1\mathcal{B}_\theta, \tag{59}$$

$$\mathcal{M}_3 = \mathcal{B}_\theta^T\mathcal{M}_2, \tag{60}$$

$$\mathcal{M}_4 = \mathcal{B}_q^T\mathcal{M}_2, \tag{61}$$

$$\mathcal{M}_5 = \mathcal{B}_q^T\mathcal{M}_1\mathcal{B}_q, \tag{62}$$

$$\mathcal{M}_6 = \mathcal{I}_{vq}^T\mathcal{P}^{-T}, \tag{63}$$

$$\mathcal{M}_7 = \mathcal{M}_6\mathcal{B}_q, \tag{64}$$

$$\mathcal{M}_8 = \mathcal{M}_6\mathcal{B}_\theta, \tag{65}$$

To this aim, suitable algorithms and data structures can be used, taking advantage of the sparse structure of the matrices.

Remark 3. When mode shapes are orthonormalized, as usually done by FEM packages,[16] an identity matrix is obtained for $\boldsymbol{M}_{e,i} = \boldsymbol{I}_i^6$, while the stiffness matrix $\boldsymbol{K}_{e,i}$ is a diagonal matrix, whose elements are the squares of mode frequencies.

2.4. Adding an external force at the tip

In order to model interactions of the end effector with external objects, the model can be extended to account for an external wrench acting at the tip of the manipulator.

If $\boldsymbol{F}_e = [\,\boldsymbol{n}_e^T \;\; \boldsymbol{f}_e^T\,]^T \in \mathbb{R}^6$ is the wrench exerted on link N at the origin of the frame $\{O'_N, \boldsymbol{x}'_N, \boldsymbol{y}'_N, \boldsymbol{z}'_N\}$, Eqs. (44) and (46) modify as it follows:

$$\mathcal{I}_{vv}\dot{\mathcal{V}} + \mathcal{I}_{vq}\ddot{\boldsymbol{q}} - \mathcal{C}_v = \mathcal{P}\mathcal{F} + \tilde{\mathcal{P}}\boldsymbol{F}_e, \tag{66}$$

$$\mathcal{I}_{vq}^T\dot{\mathcal{V}} + \mathcal{M}_e\ddot{\boldsymbol{q}} + \mathcal{D}_e\dot{\boldsymbol{q}} + \mathcal{K}_e\boldsymbol{q} - \mathcal{C}_f = -\mathcal{B}_q^T\mathcal{F} + \tilde{\mathcal{B}}_q^T\boldsymbol{F}_e, \tag{67}$$

where

$$\tilde{\mathcal{P}} = \begin{bmatrix} \boldsymbol{0} \\ \boldsymbol{0} \\ \boldsymbol{0} \\ \vdots \\ \boldsymbol{0} \\ \boldsymbol{P}_N^T \end{bmatrix} \in \mathbb{R}^{6N\times 6}, \quad \tilde{\mathcal{B}}_q^T = \begin{bmatrix} \boldsymbol{0} \\ \boldsymbol{0} \\ \boldsymbol{0} \\ \vdots \\ \boldsymbol{0} \\ \boldsymbol{B}_{q,N}^T \end{bmatrix} \in \mathbb{R}^{M\times 6} \tag{68}$$

so that the following holds:

$$\mathcal{M}_{\theta\theta}\ddot{\boldsymbol{\theta}} + \mathcal{M}_{\theta q}\ddot{\boldsymbol{q}} + \mathcal{C}_\theta = \boldsymbol{\tau} + \mathcal{B}_\theta^T\mathcal{P}^{-1}\tilde{\mathcal{P}}\boldsymbol{F}_e, \tag{69}$$

$$\mathcal{M}_{\theta q}^T\ddot{\boldsymbol{\theta}} + \mathcal{M}_{qq}\ddot{\boldsymbol{q}} + \mathcal{D}_e\dot{\boldsymbol{q}} + \mathcal{K}_e\boldsymbol{q} + \mathcal{C}_{\boldsymbol{q}} = \left(\tilde{\mathcal{B}}_q^T + \mathcal{B}_q^T\mathcal{P}^{-1}\tilde{\mathcal{P}}\right)\boldsymbol{F}_e, \tag{70}$$

2.5. Adding a payload at the tip

Assume $\{O'_N, \boldsymbol{x}'_N, \boldsymbol{y}'_N, \boldsymbol{z}'_N\}$ as the end-effector frame and model the payload as a rigid body with m_p, $\boldsymbol{I}_p$ and $\bar{\boldsymbol{r}}_p$ defining its mass, inertia tensor and vector locating its center of mass with respect to the end-effector frame respectively.

https://doi.org/10.1017/S0263574715000934 Published online by Cambridge University Press

Applying the Newton–Euler equations to the payload, considered as a floating body and subject to the wrench $-\boldsymbol{F}_e$, gives

$$\tilde{\bar{\boldsymbol{r}}}_p\dot{\bar{\boldsymbol{v}}}_p + \boldsymbol{I}_p\dot{\bar{\boldsymbol{\omega}}}_p = -\bar{\boldsymbol{\omega}}_p \times \boldsymbol{I}_p\bar{\boldsymbol{\omega}}_p - \bar{\boldsymbol{n}}_e, \tag{71}$$

$$m_p\dot{\bar{\boldsymbol{v}}}_p + \tilde{\bar{\boldsymbol{r}}}_p^T\dot{\bar{\boldsymbol{\omega}}}_p = -\bar{\boldsymbol{\omega}}_p \times \left(\bar{\boldsymbol{\omega}}_p \times \bar{\boldsymbol{r}}_p\right) - \bar{\boldsymbol{f}}_e, \tag{72}$$

and projecting the said equations on the absolute frame through the matrix $\boldsymbol{A}_p = \boldsymbol{A}_N\hat{\boldsymbol{A}}_N$, while defining $\dot{\boldsymbol{V}}_p = [\,\dot{\boldsymbol{\omega}}_p^T\ \dot{\boldsymbol{v}}_p^T\,]^T \in \mathbb{R}^6$ yields

$$\boldsymbol{F}_e = -\boldsymbol{\mathcal{I}}_{vv,p}\dot{\boldsymbol{V}}_p - \boldsymbol{\mathcal{C}}_{v,p}, \tag{73}$$

where

$$\boldsymbol{\mathcal{I}}_{vv,p} = \begin{bmatrix} \boldsymbol{A}_p\boldsymbol{I}_p\boldsymbol{A}_p^T & \boldsymbol{A}_p\tilde{\bar{\boldsymbol{r}}}_p \\ \boldsymbol{A}_p\tilde{\bar{\boldsymbol{r}}}_p^T & m_p\boldsymbol{U} \end{bmatrix}, \tag{74}$$

$$\boldsymbol{\mathcal{C}}_{v,p} = \begin{bmatrix} \boldsymbol{\omega}_p \times \boldsymbol{A}_p\boldsymbol{I}_p\boldsymbol{A}_p^T\boldsymbol{\omega}_p \\ \boldsymbol{\omega}_p \times \left(\boldsymbol{\omega}_p \times \boldsymbol{A}_p\bar{\boldsymbol{r}}_p\right) \end{bmatrix}, \tag{75}$$

Recalling that $\dot{\boldsymbol{V}}_p$ can be obtained as:

$$\dot{\boldsymbol{V}}_p = \tilde{\boldsymbol{\mathcal{P}}}^T\dot{\boldsymbol{\mathcal{V}}} + \tilde{\boldsymbol{\mathcal{B}}}_q\ddot{\boldsymbol{q}} + \dot{\boldsymbol{V}}'_{N+1} \tag{76}$$

$$\dot{\boldsymbol{V}}'_{N+1} = \begin{bmatrix} \boldsymbol{\omega}_N \times \left(\boldsymbol{A}_N\hat{\boldsymbol{S}}_N\dot{\boldsymbol{q}}_N\right), \\ \boldsymbol{\omega}_N \times \left(\boldsymbol{\omega}_N \times \boldsymbol{p}_{N+1,N} + \boldsymbol{A}_N\boldsymbol{S}_N\dot{\boldsymbol{q}}_N\right) \end{bmatrix}, \tag{77}$$

substituting (77) in (73) and (73) in (66), (67) one obtains:

$$\hat{\boldsymbol{\mathcal{I}}}_{vv}\dot{\boldsymbol{\mathcal{V}}} + \hat{\boldsymbol{\mathcal{I}}}_{vq}\ddot{\boldsymbol{q}} - \hat{\boldsymbol{\mathcal{C}}}_v = \boldsymbol{\mathcal{P}}\boldsymbol{\mathcal{F}}, \tag{78}$$

$$\hat{\boldsymbol{\mathcal{I}}}_{vq}^T\dot{\boldsymbol{\mathcal{V}}} + \hat{\boldsymbol{\mathcal{M}}}_e\ddot{\boldsymbol{q}} + \boldsymbol{\mathcal{D}}_e\dot{\boldsymbol{q}} + \boldsymbol{\mathcal{K}}_e\boldsymbol{q} - \hat{\boldsymbol{\mathcal{C}}}_f = -\boldsymbol{\mathcal{B}}_q^T\boldsymbol{\mathcal{F}}, \tag{79}$$

where

$$\hat{\boldsymbol{\mathcal{I}}}_{vv} = \boldsymbol{\mathcal{I}}_{vv} + \tilde{\boldsymbol{\mathcal{P}}}\boldsymbol{\mathcal{I}}_{vv,p}\tilde{\boldsymbol{\mathcal{P}}}^T, \tag{80}$$

$$\hat{\boldsymbol{\mathcal{I}}}_{vq} = \boldsymbol{\mathcal{I}}_{vq} + \tilde{\boldsymbol{\mathcal{P}}}\boldsymbol{\mathcal{I}}_{vv,p}\tilde{\boldsymbol{\mathcal{B}}}_q, \tag{81}$$

$$\hat{\boldsymbol{\mathcal{C}}}_v = \boldsymbol{\mathcal{C}}_v - \tilde{\boldsymbol{\mathcal{P}}}\left(\boldsymbol{\mathcal{I}}_{vv,p}\dot{\boldsymbol{V}}'_N + \boldsymbol{\mathcal{C}}_{v,p}\right), \tag{82}$$

$$\hat{\boldsymbol{\mathcal{M}}}_e = \boldsymbol{\mathcal{M}}_e + \tilde{\boldsymbol{\mathcal{B}}}_q^T\boldsymbol{\mathcal{I}}_{vv,p}\tilde{\boldsymbol{\mathcal{B}}}_q, \tag{83}$$

$$\hat{\boldsymbol{\mathcal{C}}}_f = \boldsymbol{\mathcal{C}}_f - \tilde{\boldsymbol{\mathcal{B}}}_q^T\left(\boldsymbol{\mathcal{I}}_{vv,p}\dot{\boldsymbol{V}}'_N + \boldsymbol{\mathcal{C}}_{v,p}\right), \tag{84}$$

Therefore, Eqs (1) and (2) still follow by simply replacing $\boldsymbol{\mathcal{I}}_{vv}, \boldsymbol{\mathcal{I}}_{vq}, \boldsymbol{\mathcal{C}}_v, \boldsymbol{\mathcal{M}}_e, \boldsymbol{\mathcal{C}}_f$ in (48) and (50), while (56) and (57) are replaced with $\hat{\boldsymbol{\mathcal{I}}}_{vv}, \hat{\boldsymbol{\mathcal{I}}}_{vq}, \hat{\boldsymbol{\mathcal{C}}}_v, \hat{\boldsymbol{\mathcal{M}}}_e, \hat{\boldsymbol{\mathcal{C}}}_f$.

3. Model Validation

The validation of the model has been carried out in two steps, the results obtained by implementing and simulating model (1,2) in MATLAB have been first compared with the results obtained by simulating the same system in Dymola. The chosen system is a common literature benchmark, whose dynamics and simulation results are widely known. Furthermore, model of an experimental manipulator has been implemented and the simulation has been compared with experimental results provided by the

https://doi.org/10.1017/S0263574715000934 Published online by Cambridge University Press

Table II. Slider crank data.

	Crank	Rod
Length (m)	0.152	0.304
Radius (m)	0.005	0.005
Young's modulus (N/m^2)	1×10^9	5×10^7
Density (Kg/m^3)	2767	2767

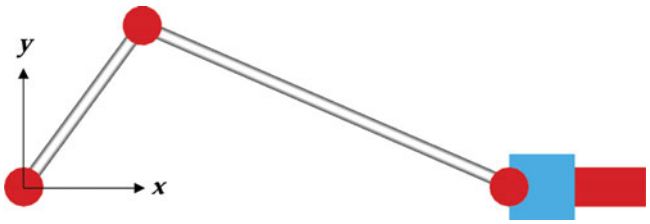


Fig. 2. Flexible slider crank.

MERIt dataset ([45]), which provides several measurements carried out on the TUDOR experimental platform, a three DOFs elastic manipulator designed by the Technische Universität Dortmund.

3.1. Simulation results

A simulation benchmark, often considered in the flexible multibody literature,[51] has been implemented, namely the simulation of a flexible slider crank mechanism (Fig. 2). The links' data (Table I) have been obtained as the result of a FE preprocessing followed by a modal reduction step,[33] performed by means of the MSC Nastran/Patran suite. The results of the modal reduction, stored in a binary file (.mnf) adopted by MSC Adams[16] for flexible multibody simulation, were first converted into an ASCII file (.mtx), and then parsed by an external tool, finally generating a HDF5 (Hierarchical Data Format 5) file. Starting from the data reported in ref. [51] and summarized in Table II, the FE model of the crank was characterized with 10 nodes and meshed with CBAR2 elements, while the rod model was characterized with 20 nodes. Twelve eigenmodes were retained in both cases.

The DASSL solver has been used in Dymola, while the `ode15s` solver has been used in MATLAB.

It must be pointed out that the prismatic joint constraining the tip of the slider to move along the $\boldsymbol{x}$ axis closes a kinematic chain, and actually defines an overall differential-algebraic equation (DAE) system. Since the simulation of this DAE system resulted very difficult to be tackled by MATLAB solvers from a numerical point of view, the kinematic constraint has been replaced by a very stiff spring-damper system, acting on the tip of the slider along the $\boldsymbol{y}$ axis, with a stiffness constant $K = 1 \times 10^5$ N/m and a damping $D = 100$ Ns/m. Figure 3 shows, the relevant Dymola model scheme.

The crankshaft was driven by the following torque:

$$\tau(t) = \begin{cases} 0.01\left[1 - \exp(-t/0.167)\right], & t \leq 0.7 \text{ s} \\ 0, & t > 0.7 \text{ s} \end{cases} \tag{85}$$

Figure 4 shows, the displacement of the slider along the $\boldsymbol{x}$ axis, obtained with the MATLAB (solid line) and Dymola (dashed line) simulation; as it is apparent, the two plots are indistinguishable. Some difference between the two simulations is appreciable in Fig. 5, where the transverse displacements of the rod center with respect to a rigid motion are shown. The results are in agreement with the benchmark reported in ref. [51]. It must be pointed out that the provided example represents a planar mechanism while the model is suited for three dimensional dynamics, but literature lacks of 3D widely used benchmarks.

3.2. Experimental results

In order to show the effectiveness of the modeling technique here proposed, we will now develop the model of the TUDOR experimental platform, a three DOFs elastic manipulator designed by the

https://doi.org/10.1017/S0263574715000934 Published online by Cambridge University Press

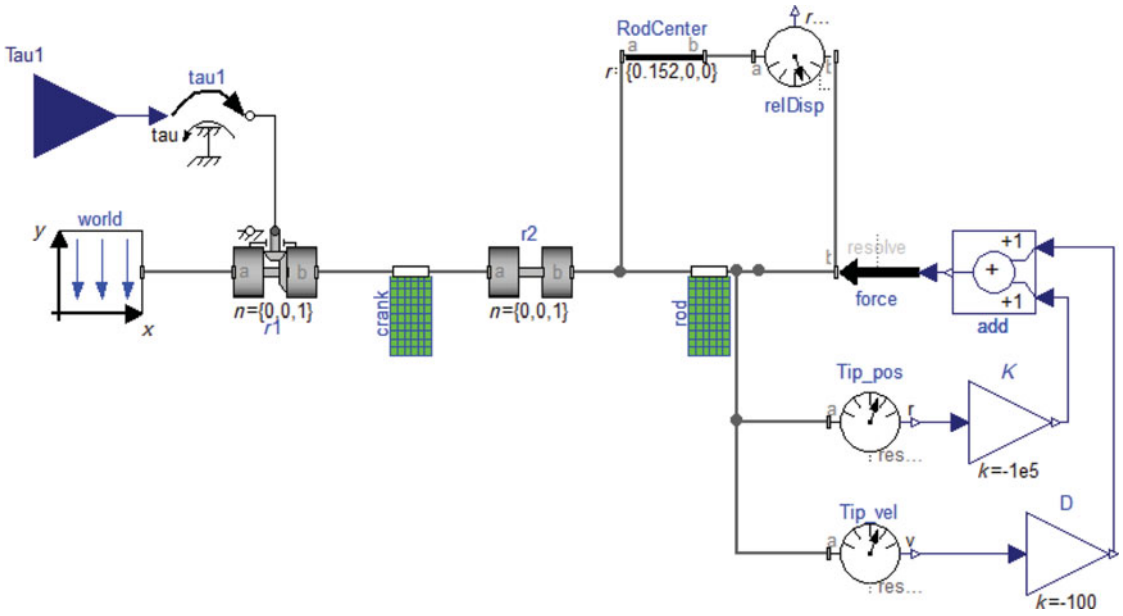


Fig. 3. Dymola model scheme of the slider crank.

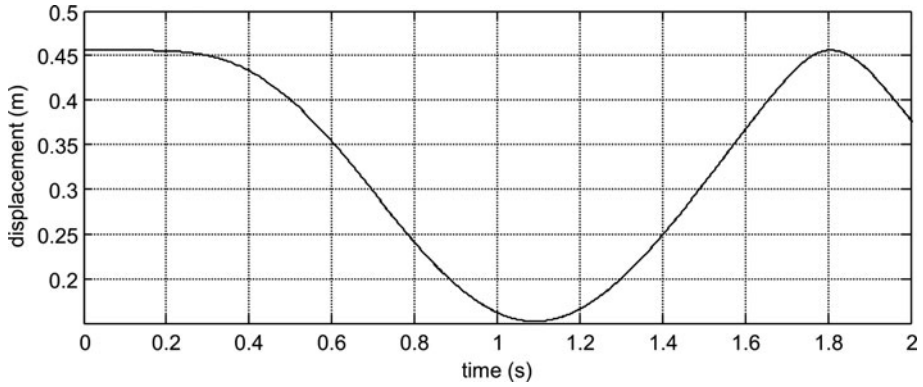


Fig. 4. Displacement of the slider along the x axis obtained with the Dymola simulation (dashed line), and with the MATLAB simulation (solid line).

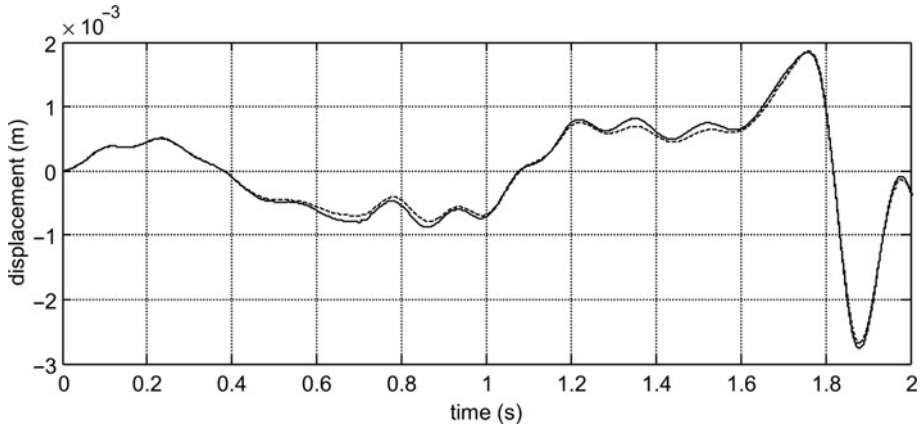


Fig. 5. Transverse displacements of the rod center with respect to a rigid motion obtained with the Dymola simulation (dashed line), and with the MATLAB simulation (solid line).

https://doi.org/10.1017/S0263574715000934 Published online by Cambridge University Press

Table III. Tudor link data.

	Link 1	Link 2
Length	440 mm	410 mm
Width	15 mm	15 mm
Height	4 mm	4 mm
Density	7800 Kg/m^3	7800 Kg/m^3
Young Modulus	200 GPa	200 GPa

Table IV. Tudor joint data.

	Joint 1	Joint 2
Motor model	EC-max40	EC-max30
Rotor and gear Inertia	9.41×10^{-6} Kgm^2	0.82×10^{-6} Kgm^2
Torque constant	44.8 mNm/A	12.9 mNm/A
Gear Ratio	320 : 1	246 : 1
Mass	1.6680 Kg	0.5885 Kg

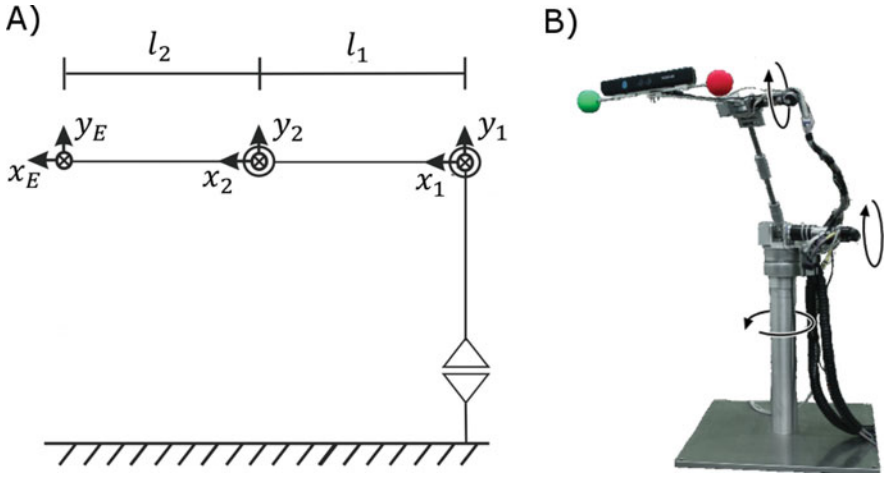


Fig. 6. Equivalent kinematic (A) and picture (B) of the robot of the TUDOR experimental platform.

Technische Universität Dortmund. The model will be then experimentally validated by means of the MERIt dataset,[45] an online available set of experimental measurements collected using TUDOR.

The equivalent kinematics of the manipulator, whose complete description can be found in ref. [52], is depicted in Fig. 6. The first link is rigid, and the first actuated joint moves the robot in the X-Z horizontal plane. Hence, in the context of this work, only the second and third links are considered, making the remaining system equivalent to a planar flexible robot. The second and third joints operate on the X-Y vertical plane, acting on joint angles θ_1 and θ_2. The manipulator kinematics is structured in order to have gravity acting on the negative Y direction. The elastic links, labeled l_1 and l_2, are constituted by spring steel rods with rectangular cross section. The rods are oriented in order to have the great flexibility in the motion plane. Links, joints and motors data are summarized in Tables III and IV.

As for the measurement system, strain gauges are placed on each elastic rod, strains are measured at 46 mm and 260 mm from the root of the first rod, and 45 mm and 235 mm from the root of the second rod. It must be considered however, that the initial part of each link is clamped due to mechanical connection to the joint. The length of the clamp along the X direction is 31 mm for the first link, and 28 mm for the second one. In Fig. 7, strain gauge positions and clamped parts are shown.

The manipulator can be equipped with a variable payload on the tip, the dataset includes experiments with different payloads, namely 0, 100, 200, 300 and 400 gr. Nine tests are provided for

https://doi.org/10.1017/S0263574715000934 Published online by Cambridge University Press

Table V. Considered eigenfrequencies.

Link 1		Link 2	
Mode number	Frequency (Hz)	Mode number	Frequency (Hz)
1	4.7	1	22.9
3	75.6	3	143.44
4	241.3	4	401.33

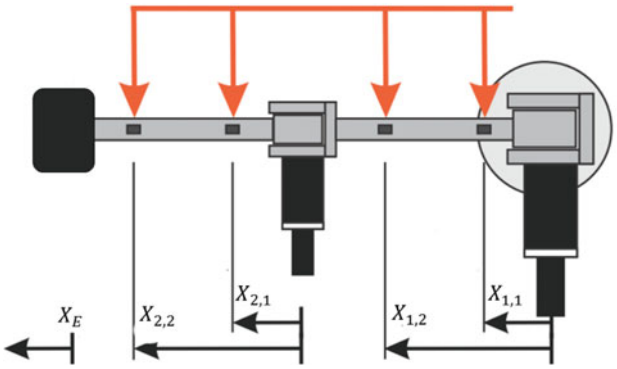


Fig. 7. Locations of the strain gauges along the robot.

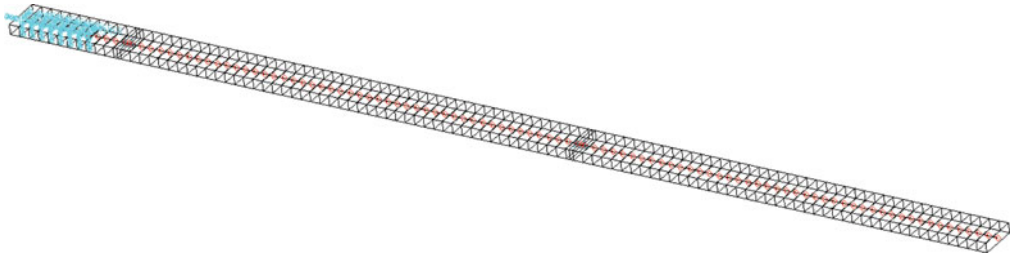


Fig. 8. Mesh of the FEM model of a link.

every payload condition and in every test, a different pseudo-random set point is generated for the joint angles θ_1 and θ_2.

Summarizing, the experimental measurements provided by the MERIt dataset are: joint angles and velocities, motor currents and the strain measured by the sensors.

Link data, summarized in Table I, have been obtained by means of a FE modal reduction stage, similarly to the data of the slider-crank mechanism outspread in the previous section.

Both links have been modeled with beam elements, as shown in Fig. 8, adopting an automatic procedure for node placement, except for the nodes corresponding to the strain sensor positions. Three nodes have been placed at a distance of 1.5 mm each, in the position corresponding to each strain gauge, in order to obtain the strain value from the nodal displacements.

For each flexible link, only three eigenmodes have been considered (see Table V), the 2nd eigenmode has been discarded, because it is a bending mode in the out-of-plane direction, where no strain gauge are present in the experimental setup. Though the number of eigenmodes is low, it has revealed adequate to correctly represent the flexible dynamics of TUDOR. An higher precision could be achieved with more eigenmodes causing, however, an increased computational burden.

The boundary conditions adopted in the FE analysis have great influence on the mode shapes of the flexible links, manipulator's links are clamped at one end, hence the nodes corresponding to the clamped part have been constrained in the FE model. Furthermore, clamping the first node of the link intrinsically guarantees that the FFR is placed in the above-mentioned node, hence the hypothesis of placing the FFR in the base flexible links is satisfied.

https://doi.org/10.1017/S0263574715000934 Published online by Cambridge University Press

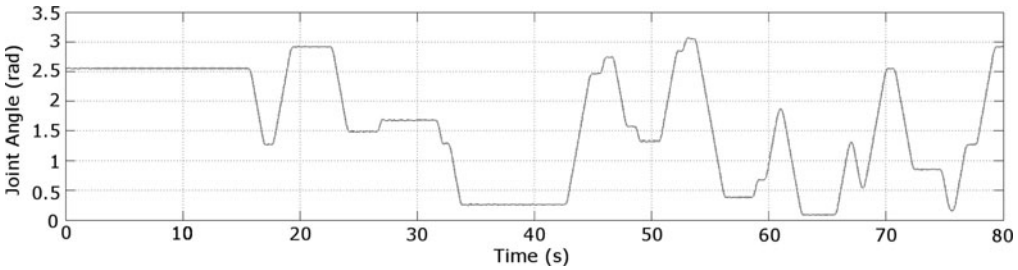


Fig. 9. First joint angle θ_1, MERIt experimental data (dashed line), and MATLAB simulation (solid line).

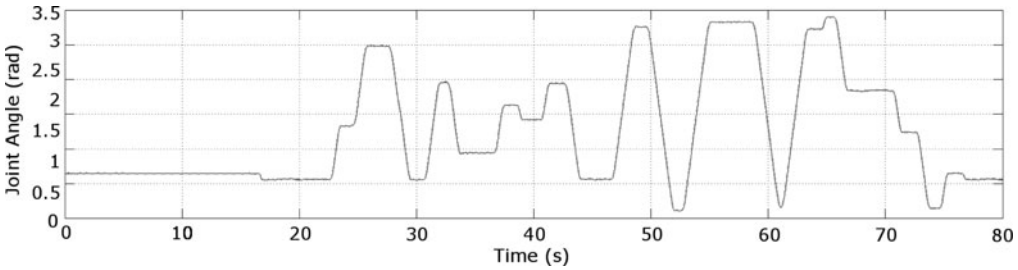


Fig. 10. Second joint angle θ_2, MERIt experimental data (dashed line), and MATLAB simulation (solid line).

The motor and gear inertia related to the actuator on θ_2 are considered in the FE modeling stage by applying a concentrated mass fixed on the first link's tip, while the payload on the manipulator's tip is considered in the closed form model.

In order to correctly simulate the motion of the manipulator, a closed-loop approach has been adopted. The commanded joint angles have been used as set points for two PID controllers that have been manually tuned with the aim of correctly reproduce the behavior of the TUDOR manipulator in terms of joint positions.

The closed loop approach has been chosen in order to compensate the effects of friction and rotary inertia, while focusing the attention on the flexible dynamics.

MERIt, includes only joint, current and link strain, no absolute or relative displacement of the links is provided. On the contrary, the model described in Section 2 determines only displacements and orientation of the nodes with respect to the FFR. Absolute nodal positions can then be computed.

In order to compare experimental results with simulations, link strains at the stain gauge positions have been derived from the nodal displacements. The beam elements are 1D from the FE perspective, hence, the strain on the surface of the beam must be computed starting from the transversal deflection. The deflection of three consecutive nodes, placed at a relative distance of 1.5 mm have been calculated by means of the $\boldsymbol{S}_i$ shape matrices. Then, recalling that the FFR presents no deflection, a cubic function $\Omega(x) = Ax^3 + Bx^2 + Cx$, describing deflection along the beam length, has been interpolated in the four nodes (FFR and three nodes around the gauge position). Finally, considering that strain is proportional to the second derivative of the deflection with respect to the beam length coordinate x, we can compute the strain $\epsilon(i)$ at point x_i along the beam as follows: $\epsilon(i) = 6Ax_i + 2B$.

For the sake of space limitation, only results related to experiments with a payload of 400 gr. are reported here. All the figures shown in this Section present a comparison between MERIt experimental data, represented by a black solid line, and simulation results, represented by a dashed grey line.

First of all, Figs. 9 and 10 report the joint angles. Though, PID position regulators have been manually tuned, the response generated by the model is so closed to the experimental one that the two curves overlap. On the other hand, concerning the validation of the flexible dynamics, it can be noticed that there is again a good accordance between the simulated model and experimental data. In particular, Figs. 11–14 show a comparison between the strain gauge measurements and the strain computed by the model, at the same positions, while Fig. 15 shows a zoom of the strain at $X_{1,1}$ in a small time window. These figures reveal that small differences between simulated and experimental data are due to the effect of material damping, which is a parameter difficult to identify

https://doi.org/10.1017/S0263574715000934 Published online by Cambridge University Press

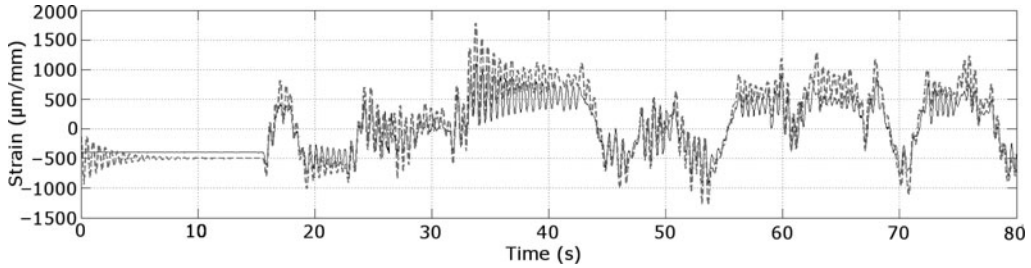


Fig. 11. Comparison between the strain gauge measurements and the strain computed by the model at the position $X_{1,1}$, MERIt experimental data (dashed line), and MATLAB simulation (solid line).

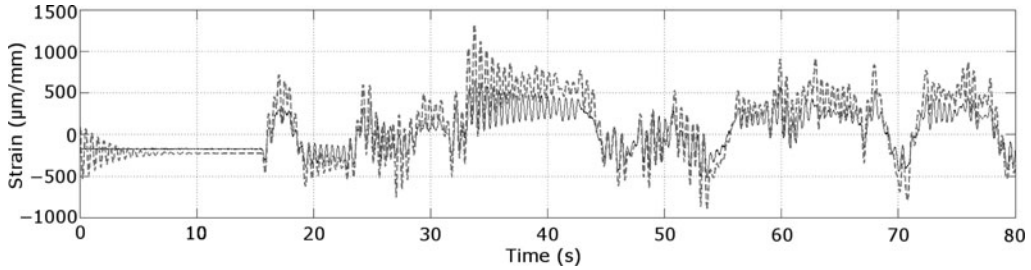


Fig. 12. Comparison between the strain gauge measurements and the strain computed by the model at the position $X_{1,2}$, MERIt experimental data (dashed line), and MATLAB simulation (solid line).

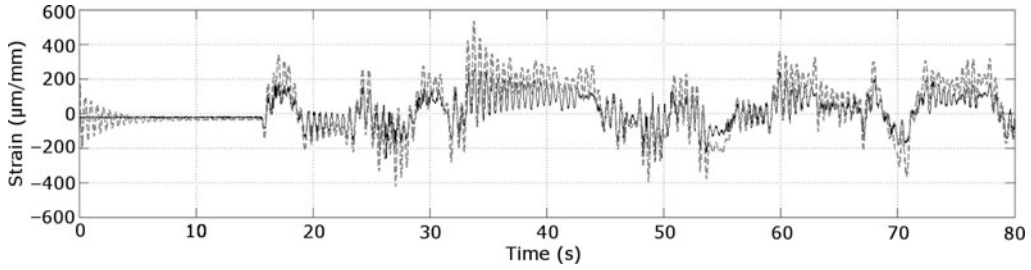


Fig. 13. Comparison between the strain gauge measurements and the strain computed by the model at the position $X_{2,1}$, MERIt experimental data (dashed line), and MATLAB simulation (solid line).

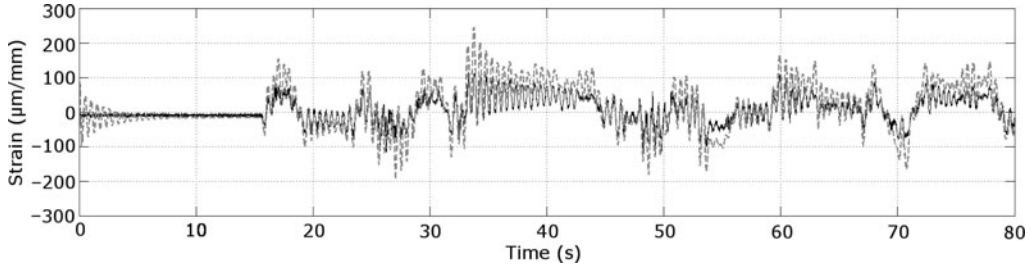


Fig. 14. Comparison between the strain gauge measurements and the strain computed by the model at the position $X_{2,2}$, MERIt experimental data (dashed line), and MATLAB simulation (solid line).

without specific experiments, and static measurement offsets, as it can be seen when the manipulator is stationary (see, e.g., the first 10 s of Fig. 11).

In order to confirm the results of the time domain analysis, a frequency analysis of the strains has been performed as well. Figures 16-19 show, a comparison between the frequency response of the strain gauge measurements and the strains computed using the model. These figures reveal, again, a good accordance between model and experimental data. In particular, a resonance around 2 Hz is shown by the simulation and experimental data as well. Strains on $X_{1,2}$ and $X_{2,2}$ for an experiment with a 200 g. payload are briefly reported in Figs. 20 and 21.

https://doi.org/10.1017/S0263574715000934 Published online by Cambridge University Press

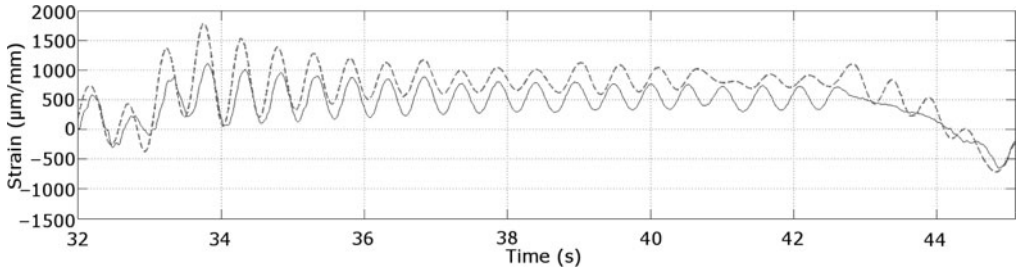


Fig. 15. Comparison between the strain gauge measurements and the strain computed by the model at the position $X_{1,1}$, MERIt experimental data (dashed line), and MATLAB simulation (solid line).

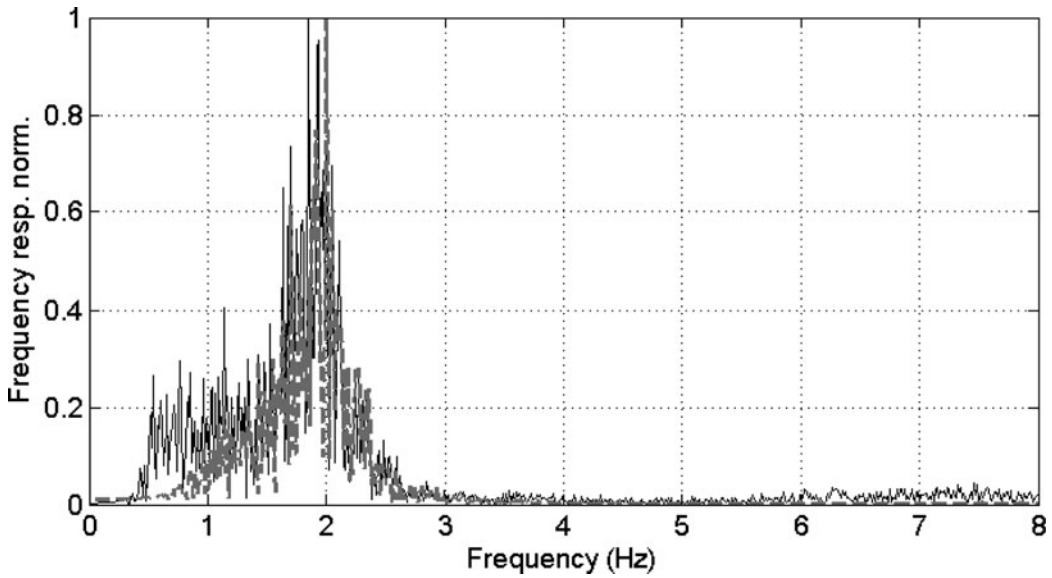


Fig. 16. Comparison between the FFT of the strain computed by the model and MERIt experimental datas at the position $X_{1,1}$, MERIt experimental data (dashed line), and MATLAB simulation (solid line).

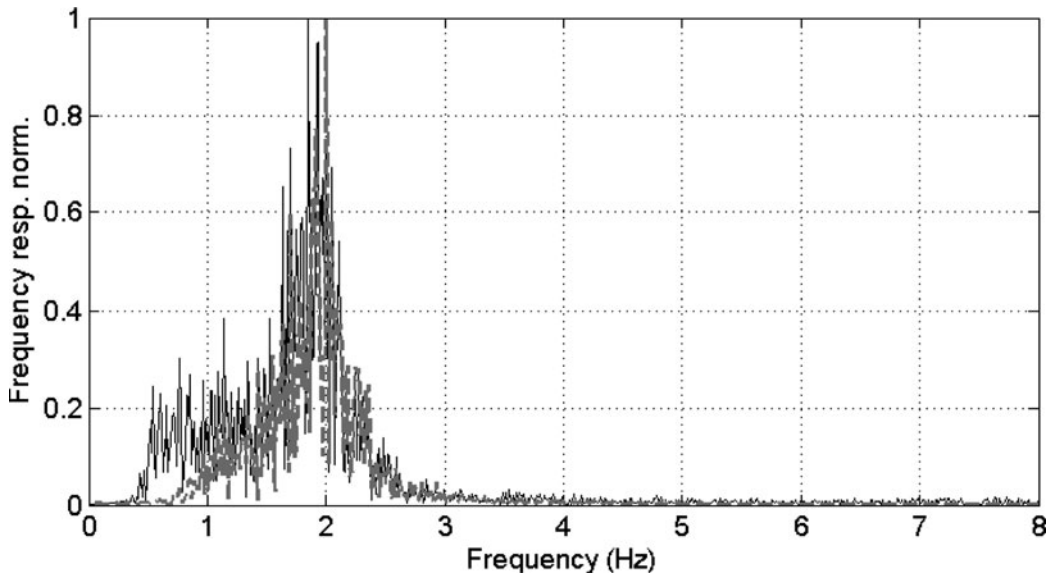


Fig. 17. Comparison between the FFT of the strain computed by the model and MERIt experimental datas at the position $X_{1,2}$, MERIt experimental data (dashed line), and MATLAB simulation (solid line).

https://doi.org/10.1017/S0263574715000934 Published online by Cambridge University Press

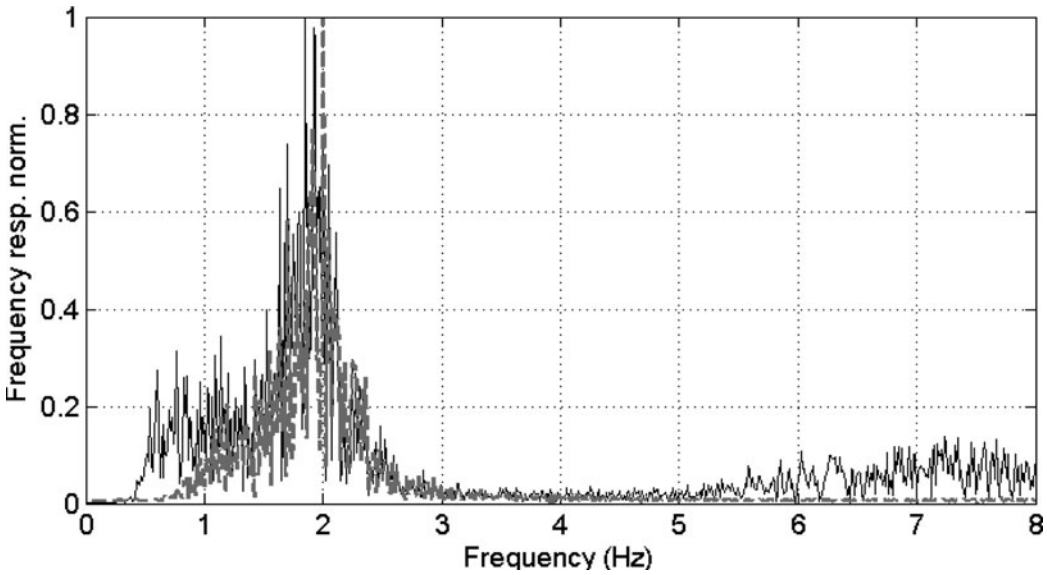


Fig. 18. Comparison between the FFT of the strain computed by the model and MERIt experimental datas at the position $X_{2,1}$, MERIt experimental data (dashed line), and MATLAB simulation (solid line).

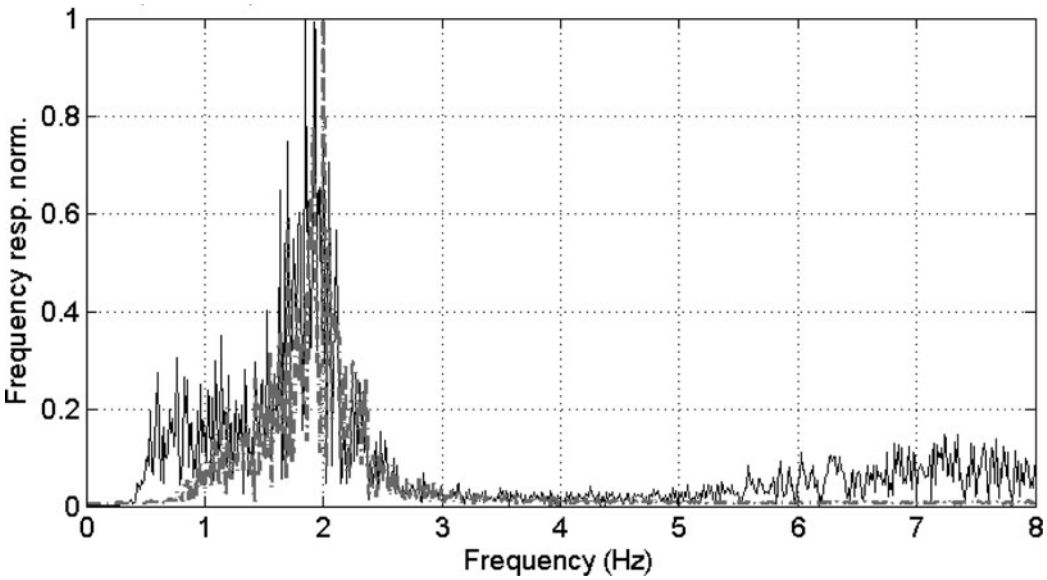


Fig. 19. Comparison between the FFT of the strain computed by the model and MERIt experimental datas at the position $X_{2,2}$, MERIt experimental data (dashed line), and MATLAB simulation (solid line).

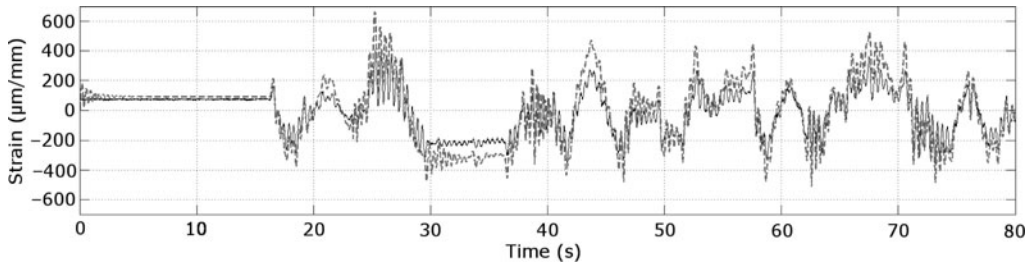


Fig. 20. Comparison between the strain gauge measurements and the strain computed by the model at the position $X_{2,1}$, MERIt experimental data (dashed line), and MATLAB simulation (solid line) - payload 200 gr.

https://doi.org/10.1017/S0263574715000934 Published online by Cambridge University Press

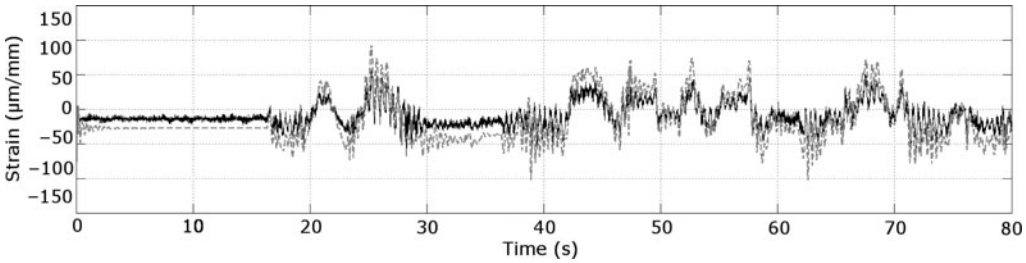


Fig. 21. Comparison between the strain gauge measurements and the strain computed by the model at the position $X_{2,2}$, MERIt experimental data (dashed line), and MATLAB simulation (solid line) - payload 200 gr.

4. Conclusion

In this paper, a closed-form 3D dynamic model of a flexible manipulator is derived with respect to the joints and the global vector of modal coordinates. The derivation is based on the adoption of the spatial vector notation, on the FFR approach, and on the Newton–Euler equations of the generic flexible body.

The parameters required by the model have been computed by means of a FE preprocessing stage, which allows to easily consider links with an arbitrary geometry.

The model has been validated by comparison of the simulation results obtained with a MATLAB implementation with the results obtained through a classical multibody modeling approach, performed in the Modelica/Dymola environment, with reference to benchmarks taken from the literature.

Then, the model of the TUDOR experimental platform, a two link flexible manipulator, has been derived and implemented. This model has been then validated using the online available experimental dataset MERIt, showing a good accordance between simulations and experiments.

The efficiency of the model can be now further improved by exploiting the sparsity of matrices, in view of a use of the model for real-time control, which appears to be the most promising next step of the research. Future developments will concern the automatic derivation from the manipulator motion equations of a two-time scale approximation, that will be then adopted as the framework to solve estimation and control problems.

Acknowledgments

The authors would like to thank sincerely J. Malzahn and T. Bertram for having publicly released the experimental data of MERit/TUDOR. This provided us with a unique opportunity to perform a thorough validation of the model, due to the lack of similar benchmarks in literature.

References

1. A. Albu-Schäffer, S. Haddadin, C. Ott, A. Stemmer, T. Wimböck and G. Hirzinger, "The DLR lightweight robot: design and control concepts for robots in human environments," *Ind. Robot: Int. J.* **34**(5), 376–385 (2007).
2. E. Baumgartner, R. Bonitz, J. Melko, L. Shiraishi and P. Leger, "The Mars Exploration Rover Instrument Positioning System," *Aerospace Conference, 2005 IEEE*, Big Sky, MT, USA (2005) pp. 1–19.
3. M. Filipović, V. Potkonjak and M. Vukobatović, "Elasticity in humanoid robotics," *Scientific Technical Review*, Military Technical Institute, Belgrade, vol. 1 (2007) pp. 24–33.
4. W. J. Book, "Recursive Lagrangian dynamics of flexible manipulator arms," *The Int. J. Robot. Res.* **3**(3), 87–101 (1984).
5. A. De Luca and B. Siciliano, "Closed-form dynamic model of planar multilink lightweight robots," *IEEE Trans. Syst. Man Cybern.* **21**(4), 826–839 (1991).
6. C. Li and T. S. Sankar, "Systematic methods for efficient modeling and dynamics computation of flexible robot manipulators," *IEEE Trans. Syst. Man Cybern.* **23**(1), 77–95 (1993).
7. W. Chen, "Dynamic modeling of multi-link flexible robotic manipulators," *Comput. Struct.* **79**(2), 183–195 (2001).
8. D. Zhang and S. Zhou, "Dynamic analysis of flexible-link and flexible-joint robots," *Appl. Math. Mech.* **27**(5), 695–704 (2006).
9. J. Qingxuan, Z. Xiaodong, S. Hanxu and C. Ming, "Active Control of Space Flexible-Joint/Flexible-Link Manipulator," *IEEE Conference on Robotics, Automation and Mechatronics*, Chengdu, China (2008) pp. 812–818.
10. W. Chen, "Dynamic modeling of multi-link flexible robotic manipulators," *Comput. Struct.* **79**(2), 183–195 (2001).

https://doi.org/10.1017/S0263574715000934 Published online by Cambridge University Press

11. J. Sadler and Z. Yang, "A comprehensive study of modal characteristics of a cylindrical manipulator with both link and joint flexibility," *Mech. Mach. Theory* **32**(8), 941–956 (1997).
12. X. Wang and J. K. Mills, "Dynamic modeling of a flexible-link planar parallel platform using a substructuring approach," *Mech. Mach. Theory* **41**(6), 671–687 (2006).
13. M. Rognant, E. Courteille and P. Maurine, "A systematic procedure for the elastodynamic modeling and identification of robot manipulators," *IEEE Trans. Robot.* **26**(6), 1085–1093 (2010).
14. R. J. Theodore and A. Ghosal, "Comparison of the assumed modes and finite element models for flexible multilink manipulators," *Int. J. Robot. Res.* **14**(2), 91–111 (1995).
15. A. Heckmann, "On the choice of boundary conditions for mode shapes in flexible multibody systems," *Multibody Syst. Dyn.* **23**(2), 141–163 (2009).
16. MSC Software Corporation, ADAMS/Flex – Theory of Flexible Bodies (2003).
17. K. Shihabudheen and J. Jacob, "Composite Control of Flexible Link Flexible Joint Manipulator," *Annual IEEE India Conference (INDICON)*, Kochi,Kerala,India (2012) pp. 827–831.
18. M. Kirćanski, M. Vukobratović, N. Kirćanski and A. Timčenko, "A new program package for the generation of efficient manipulator kinematic and dynamic equations in symbolic form," *Robotica* **6**(04), 311–318 (1988).
19. A. Mohan and S. Saha, "A recursive, numerically stable, and efficient simulation algorithm for serial robots with flexible links," *Multibody Syst. Dyn.* **21**(1), 1–35 (2009).
20. J. Hollerbach, "A recursive Lagrangian formulation of maniputator dynamics and a comparative study of dynamics formulation complexity," *IEEE Trans. Syst. Man Cybern.* **10**(11), 730–736 (1980).
21. A. A. Shabana and R. Y. Yakoub, "Three dimensional absolute nodal coordinate formulation for beam elements: Theory," *J. Mech. Des.* **123**(4), 606–613 (2000).
22. A. A. Shabana and R. Y. Yakoub, "Three dimensional absolute nodal coordinate formulation for beam elements: Implementation and applications," *Journal of Mechanical Design* **123**(4), 614–621 (2000).
23. A. Shabana and R. Schwertassek, "Equivalence of the floating frame of reference approach and finite element formulations," *Int. J. Non-Linear Mech.* **33**(3), 417–432 (1998).
24. F. Pfeiffer and B. Gebler, "A Multistage-Approach to the Dynamics and Control of Elastic Robots," *Proceedings IEEE International Conference on Robotics and Automation*, Philadelphia,PA,USA, vol. 1 (1988) pp. 2–8.
25. N. Pedersen and M. Pedersen, "A direct derivation of the equations of motion for 3d-flexible mechanical systems," *Int. J. Numer. Methods Eng.* **41**(4), 697–719 (1998).
26. T. Wasfy, "Modeling Contact/Impact of Flexible Manipulators with a Fixed Rigid Surface, *Proceedings IEEE International Conference on Robotics and Automation*, Nagoya, Japan, vol. 1 (1995) pp. 621–626.
27. M. Hermle and P. Eberhard, "Control and parameter optimization of flexible robots," *Mech. Struct. Mach.* **28**(2-3), 137–168, (2000).
28. F. Dignath, C. Breuninger, P. Eberhard and L. Kübler, "Optimization of mechatronic systems using the software package NEWOPT/AIMS," *Multibody Syst. Dyn.* **13**(1), 85–100 (2005).
29. M. Reiner, M. Otter and H. Ulbrich, "Modeling and Feed-forward Control of Structural Elastic Robots," **In**: *ICNAAM: International Conference of Numerical Analysis and Applied Mathematics* (T. E. Simos, G. Psihoyios and C. Tsitouras, eds.) vol. 1281 (AIP, Rhodes (Greece), 2010) pp. 378–381.
30. Dassault Systemès, Dassault Systèmes Simulia Corp. Abaqus Analysis Users Manual, Version 6.9. (2009).
31. Ansys Corp., Ansys Release 11.0 Documentation (2009).
32. MSC Software, MSC/NASTRAN Reference Manual, Version 68 - Lahey, Miller, et al. (1994).
33. R. R. Craig and M. C. C. Bampton, "Coupling of substructures for dynamic analyses," *AIAA J.* **6**(7), 1313–1319 (1968).
34. P. Koutsovasilis and M. Beitelschmidt, "Comparison of model reduction techniques for large mechanical systems," *Multibody Syst. Dyn.* **20**(2), 111–128 (2008).
35. M. Lehner and P. Eberhard, "A two-step approach for model reduction in flexible multibody dynamics," *Multibody Syst. Dyn.* **17**, 157–176 (2007).
36. J. Fehr and P. Eberhard, "Simulation process of flexible multibody systems with non–modal model order reduction techniques," *Multibody Syst. Dyn.* **25**, 313–334 (2011).
37. C. Nowakowski, J. Fehr, M. Fischer and P. Eberhard, "Model Order Reduction in Elastic Multibody Systems using the Floating Frame of Reference Formulation," *Proceedings of the* 7^{th} *Vienna International Conference on Mathematical Modelling – MATHMOD*, Vienna, Austria, vol. 7, part 1 (2012) pp. 40–48.
38. R. Featherstone, *Rigid Body Dynamics Algorithms* (Springer, New York, 2008).
39. R. Featherstone and D. Orin, *Springer Handbook of Robotics* (Springer, Berlin, 2008) Ch. Dynamics, pp. 35–65.
40. A. Fijany and R. Featherstone, "A new factorization of the mass matrix for optimal serial and parallel calculation of multibody dynamics," *Multibody Syst. Dyn.* **29**, 169–187 (2013).
41. F. Boyer and P. Coiffet, "Generalization of Newton-Euler model for flexible manipulators," *J. Robot. Syst.* **13**(1), 11–24 (1996).
42. A. A. Shabana, "Dynamics of flexible bodies using generalized newton-euler equations," *J. Dyn. Syst. Meas. Control* **112**(3), 496–50 (1990).
43. K. Lee, Y. Wang and G. S. Chirikjian, "O (n) mass matrix inversion for serial manipulators and polypeptide chains using lie derivatives," *Robotica* **25**(06), 739–750 (2007).

https://doi.org/10.1017/S0263574715000934 Published online by Cambridge University Press

44. F. Schiavo, L. Viganò and G. Ferretti, "Object-oriented modelling of flexible beams," *Multibody Syst. Dyn.* **15**(3), 263–286 (2006).
45. J. Malzahn and T. Bertram, *A Multi-Elastic-Link Robot Identification Dataset* (Institute of Control Theory and Systems Engineering,(RST), TU Dortmund, Germany, 2014).
46. J. Denavit and R. S. Hartenberg, "A kinematic notation for lower-pair mechanisms based on matrices," *Trans. ASME E J. Appl. Mech.* **22**, 215–221 (1955).
47. L. Meirovitch, *Analytical Methods in Vibration* (Macmillan Publishing, New York, 1967).
48. A. A. Shabana, *Dynamics of Multibody Systems* (Cambridge University Press, New York, 1998).
49. R. Schwertassek and O. Wallrapp, *Dynamik flexibler Mehrkörpersysteme* (Vieweg, Wiesbaden, 1999).
50. L. Bascetta and P. Rocco, "Modelling flexible manipulators with motors at the joints," *Math. Comput. Modelling Dyn. Syst.* **8**(2), 157–183 (2002).
51. J. Escalona, H. Hussien, and A. Shabana, "Application of the absolute nodal coordinate formulation to multibody system dynamics," *J. Sound Vib.* **214**(5), 833–851 (1998).
52. R. F. R. Malzahn and J. T. Bertram, "Dynamics Identification of a Damped Multi Elastic Link Robot Arm under Gravity," *IEEE International Conference on Robotics and Automation*, Honkong, China (2014), pp. 2170–2175.

Appendix A. Inertia Invariants

To simplify the notation, the subscript i, denoting the ith link will be dropped. Defining $\boldsymbol{S} = [\,\boldsymbol{s}_1\ \boldsymbol{s}_2\ \ldots\ \boldsymbol{s}_M\,]$ then, from the motion equations as given in ref. [48], it follows:

$$m = \int_V \rho\, \mathrm{d}V = I^1, \tag{A1}$$

$$\begin{aligned} m\tilde{\boldsymbol{d}}_C &= \int_V \rho\tilde{\boldsymbol{u}}\, \mathrm{d}V = \int_V \rho\tilde{\boldsymbol{u}}_0\, \mathrm{d}V + \int_V \rho(\widetilde{\boldsymbol{S}\boldsymbol{q}})\, \mathrm{d}V \\ &= \int_V \rho\tilde{\boldsymbol{u}}_0\, \mathrm{d}V + \sum_{i=1}^{M}\left(\int_V \rho\tilde{\boldsymbol{s}}_i\, \mathrm{d}V\right) q_i = \tilde{\boldsymbol{I}}^2 + \sum_{i=1}^{M}\tilde{\boldsymbol{I}}_i^3 q_i, \end{aligned} \tag{A2}$$

$$\begin{aligned} \bar{\boldsymbol{C}}_t^T &= \int_V \rho\boldsymbol{S}\, \mathrm{d}V = \int_V \rho\begin{bmatrix}\boldsymbol{s}_1 & \boldsymbol{s}_2 & \ldots & \boldsymbol{s}_M\end{bmatrix} \mathrm{d}V \\ &= \begin{bmatrix}\boldsymbol{I}_1^3 & \boldsymbol{I}_2^3 & \ldots & \boldsymbol{I}_M^3\end{bmatrix}, \end{aligned} \tag{A3}$$

$$\begin{aligned} \bar{\boldsymbol{C}}_r^T &= \int_V \rho\tilde{\boldsymbol{u}}\boldsymbol{S}\, \mathrm{d}V = \int_V \rho\tilde{\boldsymbol{u}}_0\boldsymbol{S}\, \mathrm{d}V + \int_V \rho(\widetilde{\boldsymbol{S}\boldsymbol{q}})\boldsymbol{S}\, \mathrm{d}V \\ &= \int_V \rho\tilde{\boldsymbol{u}}_0\boldsymbol{S}\, \mathrm{d}V + \sum_{i=1}^{M}\left(\int_V \rho\tilde{\boldsymbol{s}}_i\boldsymbol{S}\, \mathrm{d}V\right) q_i = \boldsymbol{I}^4 + \sum_{i=1}^{M}\boldsymbol{I}_i^5 q_i, \end{aligned} \tag{A4}$$

$$\boldsymbol{M}_e = \int_V \rho\boldsymbol{S}^T\boldsymbol{S}\, \mathrm{d}V = \boldsymbol{I}^6, \tag{A5}$$

$$\begin{aligned} \bar{\boldsymbol{J}} &= \int_V \rho\tilde{\boldsymbol{u}}^T\tilde{\boldsymbol{u}}\, \mathrm{d}V \\ &= \int_V \rho\tilde{\boldsymbol{u}}_0^T\tilde{\boldsymbol{u}}_0\, \mathrm{d}V + \int_V \rho\tilde{\boldsymbol{u}}_0^T(\widetilde{\boldsymbol{S}\boldsymbol{q}})\, \mathrm{d}V + \int_V \rho(\widetilde{\boldsymbol{S}\boldsymbol{q}})^T\tilde{\boldsymbol{u}}_0\, \mathrm{d}V \\ &\quad + \int_V \rho(\widetilde{\boldsymbol{S}\boldsymbol{q}})^T(\widetilde{\boldsymbol{S}\boldsymbol{q}})\, \mathrm{d}V = \int_V \rho\tilde{\boldsymbol{u}}_0^T\tilde{\boldsymbol{u}}_0\, \mathrm{d}V - \sum_{i=1}^{M}\left(\int_V \rho\tilde{\boldsymbol{s}}_i\tilde{\boldsymbol{u}}_0\, \mathrm{d}V\right) q_i \\ &\quad - \sum_{i=1}^{M}\left(\int_V \rho\tilde{\boldsymbol{u}}_0\tilde{\boldsymbol{s}}_i\, \mathrm{d}V\right) q_i - \sum_{i=1}^{M}\sum_{j=1}^{M}\left(\int_V \rho\tilde{\boldsymbol{s}}_i\tilde{\boldsymbol{s}}_j\, \mathrm{d}V\right) q_i q_j \\ &= \boldsymbol{I}^7 - \sum_{i=1}^{M}\left(\boldsymbol{I}_i^{8T} + \boldsymbol{I}_i^8\right) q_i - \sum_{i=1}^{M}\sum_{j=1}^{M}\boldsymbol{I}_{ij}^9 q_i q_j, \end{aligned} \tag{A6}$$

https://doi.org/10.1017/S0263574715000934 Published online by Cambridge University Press

Two more inertia invariants can be introduced in order to compute the vector $\boldsymbol{h}_{\omega}^{f}$ in (25), given by:[48]

$$\begin{aligned}\boldsymbol{h}_{\omega}^{f} &= -\int_V \rho \boldsymbol{S}^T \tilde{\bar{\boldsymbol{\omega}}}^2 \bar{\boldsymbol{u}}\, \mathrm{d}V - 2\int_V \rho \boldsymbol{S}^T \tilde{\bar{\boldsymbol{\omega}}} \boldsymbol{S}\dot{\boldsymbol{q}}\, \mathrm{d}V \\ &= \left(\int_V \rho \left[-\widetilde{(\bar{\boldsymbol{\omega}} \times \bar{\boldsymbol{u}})}\boldsymbol{S}\right]^T \mathrm{d}V\right)\bar{\boldsymbol{\omega}} - 2\left(\int_V \rho \boldsymbol{S}^T \tilde{\bar{\boldsymbol{\omega}}} \boldsymbol{S}\, \mathrm{d}V\right)\dot{\boldsymbol{q}},\end{aligned} \tag{A7}$$

Defining $\boldsymbol{S}^T = [\,\hat{\boldsymbol{s}}_1^T\ \hat{\boldsymbol{s}}_2^T\ \hat{\boldsymbol{s}}_3^T\,]$ one obtains:

$$\begin{aligned}\boldsymbol{h}_{\omega}^{f} = &\left(\int_V \rho \begin{bmatrix} \bar{\omega}_1 \bar{\boldsymbol{u}}^T \boldsymbol{S} - \bar{\boldsymbol{\omega}}^T \bar{u}_1 \boldsymbol{S} \\ \bar{\omega}_2 \bar{\boldsymbol{u}}^T \boldsymbol{S} - \bar{\boldsymbol{\omega}}^T \bar{u}_2 \boldsymbol{S} \\ \bar{\omega}_3 \bar{\boldsymbol{u}}^T \boldsymbol{S} - \bar{\boldsymbol{\omega}}^T \bar{u}_3 \boldsymbol{S} \end{bmatrix}^T \mathrm{d}V\right)\bar{\boldsymbol{\omega}} \\ &- 2\left(\bar{\omega}_1 \int_V \rho \left(\hat{\boldsymbol{s}}_3^T \hat{\boldsymbol{s}}_2 - \hat{\boldsymbol{s}}_2^T \hat{\boldsymbol{s}}_3\right)\, \mathrm{d}V\right)\dot{\boldsymbol{q}} \\ &- 2\left(\bar{\omega}_2 \int_V \rho \left(\hat{\boldsymbol{s}}_1^T \hat{\boldsymbol{s}}_3 - \hat{\boldsymbol{s}}_3^T \hat{\boldsymbol{s}}_1\right)\, \mathrm{d}V\right)\dot{\boldsymbol{q}} \\ &- 2\left(\bar{\omega}_3 \int_V \rho \left(\hat{\boldsymbol{s}}_2^T \hat{\boldsymbol{s}}_1 - \hat{\boldsymbol{s}}_1^T \hat{\boldsymbol{s}}_2\right)\, \mathrm{d}V\right)\dot{\boldsymbol{q}},\end{aligned} \tag{A8}$$

which yields (35) defining ($i, j = 1, 2, 3$)

$$\boldsymbol{D}_i = \begin{bmatrix} \boldsymbol{d}_{i1} \\ \boldsymbol{d}_{i2} \\ \boldsymbol{d}_{i3} \end{bmatrix} = \int_V \rho \bar{u}_i \boldsymbol{S}\, \mathrm{d}V, \qquad \boldsymbol{I}_{ij}^{11} = \int_V \rho \hat{\boldsymbol{s}}_i^T \hat{\boldsymbol{s}}_j\, \mathrm{d}V, \tag{A9}$$

In turn, matrix $\boldsymbol{D}_i$ is given by ($i = 1, 2, 3$):

$$\begin{aligned}\boldsymbol{D}_i &= \int_V \rho \bar{u}_i \boldsymbol{S}\, \mathrm{d}V = \int_V \rho \left(\bar{\boldsymbol{u}}_0 + \boldsymbol{S}\boldsymbol{q}\right)_i \boldsymbol{S}\, \mathrm{d}V \\ &= \int_V \rho \bar{u}_{0i} \boldsymbol{S}\, \mathrm{d}V + \int_V \rho \left(\boldsymbol{S}\boldsymbol{q}\right)_i \boldsymbol{S}\, \mathrm{d}V = \begin{bmatrix} \boldsymbol{I}_{i1}^{10} \\ \boldsymbol{I}_{i2}^{10} \\ \boldsymbol{I}_{i3}^{10} \end{bmatrix} + \int_V \rho \hat{\boldsymbol{s}}_i \boldsymbol{q} \boldsymbol{S}\, \mathrm{d}V \\ &= \begin{bmatrix} \boldsymbol{I}_{i1}^{10} \\ \boldsymbol{I}_{i2}^{10} \\ \boldsymbol{I}_{i3}^{10} \end{bmatrix} + \int_V \rho \boldsymbol{q}^T \hat{\boldsymbol{s}}_i^T \boldsymbol{S}\, \mathrm{d}V = \begin{bmatrix} \boldsymbol{I}_{i1}^{10} \\ \boldsymbol{I}_{i2}^{10} \\ \boldsymbol{I}_{i3}^{10} \end{bmatrix} + \begin{bmatrix} \boldsymbol{q}^T \boldsymbol{I}_{i1}^{11} \\ \boldsymbol{q}^T \boldsymbol{I}_{i2}^{11} \\ \boldsymbol{q}^T \boldsymbol{I}_{i3}^{11} \end{bmatrix},\end{aligned} \tag{A10}$$

where $(\boldsymbol{v})_i$ is the ith element of vector $\boldsymbol{v}$ and

$$\begin{bmatrix} \boldsymbol{I}_{i1}^{10} \\ \boldsymbol{I}_{i2}^{10} \\ \boldsymbol{I}_{i3}^{10} \end{bmatrix} = \int_V \rho \bar{u}_{0i} \boldsymbol{S}\, \mathrm{d}V \qquad i = 1, 2, 3 \tag{A11}$$

https://doi.org/10.1017/S0263574715000934 Published online by Cambridge University Press

Invariants $\boldsymbol{I}_{ij}^{10}$ and $\boldsymbol{I}_{ij}^{11}$ may be however computed from invariants $\boldsymbol{I}_{i}^{8}$ and $\boldsymbol{I}_{ij}^{9}$. In fact, recalling that

$$\boldsymbol{I}_{i}^{8} = \int_{V} \rho \begin{bmatrix} -\bar{u}_{03}s_{3i} - \bar{u}_{02}s_{2i} & \bar{u}_{02}s_{1i} & \bar{u}_{03}s_{1i} \\ \bar{u}_{01}s_{2i} & -\bar{u}_{03}s_{3i} - \bar{u}_{01}s_{1i} & \bar{u}_{03}s_{2i} \\ \bar{u}_{01}s_{3i} & \bar{u}_{02}s_{3i} & -\bar{u}_{02}s_{2i} - \bar{u}_{01}s_{1i} \end{bmatrix} \mathrm{d}V, \tag{A12}$$

$$\boldsymbol{I}_{ij}^{9} = \int_{V} \rho \begin{bmatrix} -s_{3i}s_{3j} - s_{2i}s_{2j} & s_{2i}s_{1j} & s_{3i}s_{1j} \\ s_{1i}s_{2j} & -s_{3i}s_{3j} - s_{1i}s_{1j} & s_{3i}s_{2j} \\ s_{1i}s_{3j} & s_{2i}s_{3j} & -s_{2i}s_{2j} - s_{1i}s_{1j} \end{bmatrix} \mathrm{d}V, \tag{A13}$$

one obtains ($k, l = 1, \ldots, M$)

$$\left(\boldsymbol{I}_{ij}^{10}\right)_{k} = \begin{cases} \left(\boldsymbol{I}_{k}^{8}\right)_{ji} & i \neq j = 1, 2, 3 \\ \frac{1}{2}\left[\left(\boldsymbol{I}_{k}^{8}\right)_{ii} - \left(\boldsymbol{I}_{k}^{8}\right)_{mm} - \left(\boldsymbol{I}_{k}^{8}\right)_{nn}\right] & \begin{matrix} i = j = 1, 2, 3 \\ m, n = 1, 2, 3 \end{matrix} \end{cases} \tag{A14}$$

$$\left(\boldsymbol{I}_{ij}^{11}\right)_{kl} = \begin{cases} \left(\boldsymbol{I}_{kl}^{9}\right)_{ji} & i \neq j = 1, 2, 3 \\ \frac{1}{2}\left[\left(\boldsymbol{I}_{kl}^{9}\right)_{ii} - \left(\boldsymbol{I}_{kl}^{9}\right)_{mm} - \left(\boldsymbol{I}_{kl}^{9}\right)_{nn}\right] & \begin{matrix} i = j = 1, 2, 3 \\ m, n = 1, 2, 3 \end{matrix} \end{cases} \tag{A15}$$

https://doi.org/10.1017/S0263574715000934 Published online by Cambridge University Press